JGP Journal of General Physiology

RESEARCH ARTICLE

Glucose stimulates somatostatin secretion in pancreatic δ-cells by cAMP-dependent intracellular Ca^{2+} release

Geoffrey Denwood[1]*, Andrei Tarasov[1,5]*, Albert Salehi[2], Elisa Vergari[1], Reshma Ramracheya[1], Harumi Takahashi[3], Viacheslav O. Nikolaev[6], Susumo Seino[3], Fiona Gribble[4], Frank Reimann[4], Patrik Rorsman[1,2], and Quan Zhang[1]

Somatostatin secretion from pancreatic islet δ-cells is stimulated by elevated glucose levels, but the underlying mechanisms have only partially been elucidated. Here we show that glucose-induced somatostatin secretion (GISS) involves both membrane potential-dependent and -independent pathways. Although glucose-induced electrical activity triggers somatostatin release, the sugar also stimulates GISS via a cAMP-dependent stimulation of CICR and exocytosis of somatostatin. The latter effect is more quantitatively important and in mouse islets depolarized by 70 mM extracellular K^+, increasing glucose from 1 mM to 20 mM produced an ∼3.5-fold stimulation of somatostatin secretion, an effect that was mimicked by the application of the adenylyl cyclase activator forskolin. Inhibiting cAMP-dependent pathways with PKI or ESI-05, which inhibit PKA and exchange protein directly activated by cAMP 2 (Epac2), respectively, reduced glucose/forskolin-induced somatostatin secretion. Ryanodine produced a similar effect that was not additive to that of the PKA or Epac2 inhibitors. Intracellular application of cAMP produced a concentration-dependent stimulation of somatostatin exocytosis and elevation of cytoplasmic Ca^{2+} ($[Ca^{2+}]_i$). Both effects were inhibited by ESI-05 and thapsigargin (an inhibitor of SERCA). By contrast, inhibition of PKA suppressed δ-cell exocytosis without affecting $[Ca^{2+}]_i$. Simultaneous recordings of electrical activity and $[Ca^{2+}]_i$ in δ-cells expressing the genetically encoded Ca^{2+} indicator GCaMP3 revealed that the majority of glucose-induced $[Ca^{2+}]_i$ spikes did not correlate with δ-cell electrical activity but instead reflected Ca^{2+} release from the ER. These spontaneous $[Ca^{2+}]_i$ spikes are resistant to PKI but sensitive to ESI-05 or thapsigargin. We propose that cAMP links an increase in plasma glucose to stimulation of somatostatin secretion by promoting CICR, thus evoking exocytosis of somatostatin-containing secretory vesicles in the δ-cell.

Introduction

Pancreatic islets play a central role in metabolic homeostasis by secreting insulin and glucagon, the body's two principal glucoregulatory hormones. Insulin, released from pancreatic β-cells in response to elevated plasma glucose, is the only hormone capable of lowering blood glucose (Rorsman and Renström, 2003). Glucagon, released by the pancreatic α-cells in response to hypoglycemia and adrenaline, is the principal plasma glucose–increasing hormone (Gylfe and Gilon, 2014; Rorsman et al., 2014). Somatostatin, secreted by pancreatic δ-cells when glucose is elevated (Hauge-Evans et al., 2009), is a powerful paracrine inhibitor of both insulin and glucagon secretion (Cejvan et al., 2003; Hauge-Evans et al., 2009; Cheng-Xue et al., 2013), and there is circumstantial evidence that aberrant somatostatin secretion contributes to the hormone secretion defects associated with diabetes (Yue et al., 2012; Li et al., 2017). However, the cellular regulation of somatostatin secretion remains poorly understood. This is because δ-cells comprise only 5% of the islet cells (Brissova et al., 2005), making them difficult to isolate and study.

We previously proposed that CICR accounts for ∼80% of glucose-induced somatostatin secretion (GISS) and is triggered by Ca^{2+} influx through R-type Ca^{2+} channels during electrical activity, which activates RYR3 Ca^{2+}-releasing channels (Zhang et al., 2007). Interestingly, membrane depolarization per se was found to be a weak stimulus of somatostatin secretion in the absence of glucose,

[1]Oxford Centre for Diabetes, Endocrinology and Metabolism, University of Oxford, Churchill Hospital, Oxford, UK; [2]Institute of Neuroscience and Physiology, Department of Physiology, Metabolic Research Unit, University of Goteborg, Göteborg, Sweden; [3]Division of Molecular and Metabolic Medicine, Kobe University Graduate School of Medicine, Kobe, Japan; [4]Institute of Metabolic Science, University of Cambridge, Addenbrook's Hospital, Cambridge, UK; [5]School of Life and Medical Sciences, University of Hertfordshire, Hatfield, UK; [6]Institute of Experimental Cardiovascular Research, University Medical Center Hamburg-Eppendorf, Hamburg, Germany.

*G. Denwood and A. Tarasov contributed equally to this paper; Correspondence to Quan Zhang: quan.zhang@ocdem.ox.ac.uk.

indicating that glucose somehow regulates CICR. However, the identity of the intracellular coregulator of CICR is unknown. Here we propose that cAMP represents this elusive intracellular regulator, and we have dissected the major cAMP-dependent molecular signaling pathways in the regulation of somatostatin secretion.

Materials and methods

Animals and isolation of pancreatic islets

All animal experiments were conducted in accordance with the UK Animals Scientific Procedures Act (1986) and the University of Oxford ethical guidelines. Mice were killed by a Schedule 1 procedure (cervical dislocation) and the pancreases quickly resected following intraductal injection with 0.1 mg/ml liberase (TL research grade; Roche) dissolved in Hank's buffer (Sigma-Aldrich). Islets were then isolated by liberase digestion at 37°C before being hand picked and placed into culture medium (RPMI-1640; Gibco). The secretion studies and most of the electrophysiology experiments were performed on islets isolated from NMRI mice (Charles River Laboratories). A subset of the electrophysiology and Ca^{2+} imaging experiments were performed on islets from mice expressing a Cre reporter from the Rosa26 locus, either the fluorescent protein tdRFP or the genetically encoded Ca^{2+} indicator GCaMP3, conditionally activated by iCre recombinase expressed under the control of the somatostatin (SST) promoter (Chera et al., 2014; Zhang et al., 2014b; Adriaenssens et al., 2016). These mice are referred to as SST-tdRFP and SST-GCaMP3 in the text, respectively, and were bred as reported previously (Adriaenssens et al., 2015). Mice lacking exchange protein directly activated by cAMP 2 ($Epac2^{-/-}$) were generated as described elsewhere (Shibasaki et al., 2007).

Electrophysiology and capacitance measurements of exocytosis

All electrophysiological measurements were performed using an EPC-10 patch clamp amplifier and Pulse software (version 8.80; HEKA Electronics). Electrical activity, membrane currents, and changes in cell capacitance (reflecting exocytosis) were recorded from superficial δ-cells in intact, freshly isolated mouse pancreatic islets (Göpel et al., 1999, 2004) using the perforated patch or standard whole-cell techniques as indicated in the text and/or figure legends. The δ-cells were first identified by immunocytochemistry (Zhang et al., 2007), subsequently by electrophysiological fingerprinting (Briant et al., 2017), and most recently via expression of fluorescent reporters under the control of the somatostatin promoter as delineated above.

For experiments that required cells to be metabolically intact (recordings in Fig. 1, A and D; Fig. 6, A and B; Fig. 7 E; Fig. 9, C and D; Fig. 12; Fig. 13; and Fig. 14), the perforated patch technique was used. The pipette solution contained (in mM) 76 K_2SO_4, 10 NaCl, 10 KCl, 1 $MgCl_2$, and 5 HEPES (pH 7.35 with KOH). Membrane perforation was achieved by inclusion of amphotericin B (0.24 mg/ml) or gramicidin D (20 µg/ml) in the pipette-filling solution. The extracellular solution consisted of (in mM) 140 NaCl, 3.6 KCl, 0.5 $MgSO_4$, 1.5 $CaCl_2$, 0.5 NaH_2PO_4, 5 $NaHCO_3$, and 10 HEPES (pH 7.4 with NaOH). Glucose, mannoheptulose (Sigma-Aldrich), depolarizing concentration of K^+, tolbutamide, and forskolin were included in the extracellular solutions at the indicated concentrations.

Electrophysiological properties were almost identical in δ-cells of wild-type animals (n = 6 from five animals) and δ-cells expressing fluorescent reporters (tdRFP or GCaMP3, n = 3 from three animals and n = 4 from four animals, respectively; Table 1). Therefore, data from δ-cells identified by the different methods were pooled (n = 13) for statistical analysis.

Exocytosis was detected as changes in cell capacitance, which were estimated by the Lindau-Neher technique implementing the "Sine+DC" feature of the lock-in module of the Pulse software. The amplitude of the sine wave was 20 mV, and the frequency was 1,250 Hz (Kanno et al., 2004). The pipette solution dialyzing the cell interior contained (in mM) 125 Cs-glutamate, 10 CsCl, 10 NaCl, 1 $MgCl_2$, 0.05 EGTA (or indo-1 for theintracellular free Ca^{2+} concentration {$[Ca^{2+}]_i$} measurements), 3 Mg-ATP, and 5 HEPES (pH 7.1 using CsOH). cAMP, myristoylated PKI 14–22 amide (PKI, a PKA inhibitor; Tocris), and ESI-05 (4-methylphenyl-2,4,6-trimethylphenysulfone, an Epac-2 inhibitor, BioLog) were included in the intracellular (pipette-filling) solutions as indicated. For the capacitance measurements with Ca^{2+} infusion (Fig. 9, A and B), the pipette solution contained (in mM) 110 Cs-glutamate, 10 KCl, 10 NaCl, 1 $MgCl_2$, 3 MgATP, 5 HEPES, and 10 EGTA with either 3 or 5 $CaCl_2$ to achieve the free $[Ca^{2+}]_i$ of 103 nM or 240 nM, respectively (pH 7.15 with CsOH). After establishment of the whole-cell configuration, a 5-min wash-in period was allowed to "clamp" the $[Ca^{2+}]_i$ in cells that were voltage-clamped at −70 mV before commencing the electrical stimulation. The standard extracellular medium used for the capacitance measurements consisted of (in mM) 118 NaCl, 20 tetraethylammonium-Cl (to block outward K^+-currents), 5.6 KCl, 1.2 $MgCl_2$, 5 HEPES, 2.6 $CaCl_2$, and 1 D-glucose (pH 7.4 with NaOH).

For unknown reasons, the δ-cell exocytotic response to a 500-ms depolarization to 0 mV in the presence of cAMP was 50% lower in islets from SST-tdRFP mice (87 ± 21 fF, n = 16 cells from seven animals) than in islets from NMRI mice (187 ± 22 fF, n = 15 cells from 12 animals; $P < 0.05$). For this reason, the analyses in Figs. 6, 7, 8, 9, 10, and 11 are restricted to δ-cells identified by immunocytochemistry after the electrophysiological measurements.

Patch pipettes were pulled from borosilicate glass with resistances of ∼5 MΩ when filled with the pipette solutions. Standard whole-cell configuration was achieved by rupturing the cell membrane included in the patching electrode (with series resistance of <30 MΩ). All electrophysiological measurements were performed at 32–34°C.

$[Ca^{2+}]_i$ measurements and imaging

For data in Fig. 7, A–D; Fig. 8; Fig. 10; and Fig. 11 A, $[Ca^{2+}]_i$ was monitored using the ratiometric indicator indo-1 and a Photon Technology International RM-2/2005 fluorescence microfluorimetry system mounted on a Nikon E600FN upright microscope. The fluorophore was excited at 360 nm and the emitted light, after being split by a dichroic mirror, was detected by two parallel photomultipliers at 405 and 485 nm, respectively. The standard whole-cell configuration was used, with EGTA equimolarly replaced by indo-1. During these experiments, the islets were exposed to 1 mM glucose. Signal

Table 1. **Electrical activity of δ-cells measured in islets from different mouse models**

	1 mM glucose			10 mM glucose			0.2 mM tolbutamide		
	V_m (mV)	V_{peak} (mV)	Frequency (Hz)	V_m (mV)	V_{peak} (mV)	Frequency (Hz)	V_m (mV)	V_{peak} (mV)	Frequency (Hz)
NMRI (n = 6)	−71 ± 3	n/a	n/a	−54 ± 3[a]	6 ± 4	0.6 ± 0.2	−48 ± 3[b]	4 ± 3[b]	0.6 ± 0.1
SST-tdRFP (n = 3)	−74 ± 4	n/a	n/a	−62 ± 2[a]	14 ± 8	0.2 ± 0.2	−54 ± 3[b]	3 ± 3[b]	0.3 ± 02
SST-GCaMP3 (n = 4)	−73 ± 3	n/a	n/a	−54 ± 3[a]	25 ± 8	0.6 ± 0.3	−37 ± 2[b]	8 ± 4[b]	0.4 ± 0.3

Electrical activity recorded from δ-cells in intact islets isolated from NMRI, SST-tdRFP, and SST-GCaMP3 mice. Membrane potential (V_m), V_{peak}, and firing frequency of action potentials when δ-cells were exposed to 1 mM glucose, 10 mM glucose, or 200 µM tolbutamide are summarized and compared between different mouse strains. Data are presented as mean values ± SEM of indicated number of independent experiments (n) from three to five animals. No action potential was detected at 1 mM glucose in all groups. Therefore the data for V_{peak} and Frequency at 1 mM glucose are shown as n/a (not available). There were no statistical differences between the different mouse models. All the measurements were made using perforated patch clamping technique.
[a]P < 0.05 vs. 1 mM glucose (for each model).
[b]P < 0.05 vs. 20 mM glucose (for each model).

processing was performed online using Felix software (version 1.2; Photon Technology International). The background signal was measured at each wavelength before establishment of the whole-cell configuration and subtracted from the experimental values. The system was calibrated by using a series of intracellular solutions containing different concentrations of Ca^{2+} (obtained by mixing different concentrations of $CaCl_2$ and EGTA). The values of R_{min} (fluorescence ratio in the absence of Ca^{2+}, 1.35), R_{max} (fluorescence ratio at saturating $[Ca^{2+}]_i$, 5.03), and K_d (178.5) thus derived were fed into the Felix software to convert the measured F_{405}/F_{485} ratio to the $[Ca^{2+}]_i$. Baseline correction, data analysis, and presentation were performed using Clampfit (version 9.2.0.11; Molecular Devices).

For data in Fig. 5, $[Ca^{2+}]_i$ dynamics was measured by changes in fluorescence of GCaMP3 ($\Delta F/F_o$, fluorescence intensity normalized to basal) specifically expressed in δ-cells (from SST-GCaMP3 mice). The experiments were conducted using an upright Zeiss Axioskop 2FS microscope equipped with the Zeiss 510-META laser scanning system. GCaMP3 was excited by a 488-nm laser and emitted light was collected at 510 nm. Images were taken every 3 s using the ZenBlue software (Carl Zeiss). Data were analyzed using Fiji imaging processing package (National Institutes of Health).

For data in Fig. 7 E, Fig. 9, C and D, Fig. 12, Fig. 13, and Fig. 14, $[Ca^{2+}]_i$ dynamics were also reported by changes in fluorescence of GCaMP3 ($\Delta F/F_o$) in δ-cells from SST-GCaMP3 mice. The experimental settings were identical to the ones used for indo-1 measurement, but GCaMP3 was excited at 480 nm using a light-emitting diode source (wLS LED Illumination Unit; QImaging). The emitted light passed through a FITC filter set (dichromic mirror 505 and barrier filter 535/45; Nikon, Japan) and was captured by a scientific Complementary Metal-Oxide-Semiconductors (CMOS) camera (OptiMOS, QImaging). To ascertain that $[Ca^{2+}]_i$ and electrical activity were recorded from the same cell, a 500-ms voltage-clamp depolarization from −70 mV to 0 mV was applied first to elicit a transient increase in GCaMP3 fluorescence. The time-lapse image series were recorded using the Micro-Manager software (Ron Vale laboratory, University of California, San Francisco) at a frequency of 1 Hz. Synchronization of imaging acquisition and electrophysiology recordings was achieved by a TTL (Transistor-Transistor Logic) trigger signal produced by the sCMOS camera. Imaging data were analyzed using the Fiji image processing package, and baseline correction was performed using Clampfit.

The inositol triphosphate ($InsP_3$) uncaging experiments (Fig. 6, C–F) were performed using a BioRad Radiance 2100 scanning laser confocal system mounted on a Nikon Eclipse E600FN upright microscope. The recordings were performed using standard whole-cell configuration (series resistance < 30 MΩ) with the pipette solutions supplemented with 25 µM Fluo-4 (Thermo Fisher Scientific) and 50 µM caged $InsP_3$ precursor (Calbiochem). Liberation of $InsP_3$ was achieved by delivering a pulse of UV light flash (JML-C2; Rapp OptoElectronic). $[Ca^{2+}]_i$ was monitored as changes in intensity of Fluo-4 fluorescence (ΔF). Fluo-4 was excited by a 488-nm laser with emitted light collected at 510-nm wavelength. Simultaneously with the measurements of $[Ca^{2+}]_i$, cell exocytosis was monitored as increases in cell capacitance (ΔC_m) by the Pulse software.

All $[Ca^{2+}]_i$ measurement/imaging experiments were conducted at 32–34°C.

Somatostatin release

Somatostatin secretion was measured in static incubations essentially as previously described (Zhang et al., 2007; Braun et al., 2009). Briefly, freshly isolated islets were preincubated for 30 min at 37°C in Krebs–Ringer buffer consisting of (in mM) 140 NaCl, 3.6 KCl, 0.5 $MgSO_4$, 2.6 $CaCl_2$, 0.5 NaH_2PO_4, 2 $NaHCO_3$, 1 glucose, and 5 HEPES (pH 7.4 with NaOH). For secretion triggered by supraphysiological concentration of extracellular K^+ ($[K^+]_o$; data in Fig. 1 C and Fig. 4), the KCl concentration was increased to 70 mM (the NaCl concentration was correspondingly reduced to maintain iso-osmolality; ∼300 milliosmoles/l). For glucose-stimulated somatostatin secretion, 10 mM or 20 mM glucose was included in the testing buffer. A previous study (Walker et al., 2011) indicated that the two concentrations stimulate somatostatin secretion to a similar extent. Groups of 10–20 islets were then incubated for 60 min at 37°C in 1 ml of solution supplemented as indicated in the figure legends. Immediately after incubation, an aliquot of the medium was removed for determination of somatostatin concentration using a commercial radioimmunoassay (Diasource).

Measurements of islet cAMP content

Freshly isolated islets were preincubated for 2 h at 37°C in RPMI containing no glucose and supplemented with 0.05% BSA. The supernatant was discarded, and the islets were incubated at 37°C for 30 min in 1 ml of Krebs–Ringer buffer solution containing 0.05% BSA, 1 mM glucose, and 100 µM isobutyl methylxanthine, supplemented with tolbutamide (200 µM). Islets were also incubated in the presence of 1 or 10 mM glucose (no tolbutamide but with isobutyl methylxanthine). cAMP was extracted by adding 400 µl of ice-cold Na^+-acetate buffer (50 mM, pH 6.2) to the islets. The pelleted samples were boiled for 10 min and sonicated on ice before being stored at −80°C. cAMP levels were determined using a commercial radioimmunoassay (Amersham Pharmacia Biotech). Aliquots of the supernatant were removed from the same experiments for somatostatin measurements.

Measurements of cytoplasmic cAMP levels

The effects of forskolin and glucose on cytoplasmic cAMP levels ($[cAMP]_i$) in pancreatic islet cells were studied using a recombinant FRET sensor Epac2-camps (Nikolaev et al., 2004). Islets isolated from SST-tdRFP mice were dispersed into single-cell suspension before being plated on glass coverslips. Epac2-camps was delivered via adenoviral infection (10^4 units per cell). The imaging experiments were performed 36–48 h after infection using a Zeiss Axioskop 2FS microscope equipped with a 40×/1.3 objective, a Lambda DG-4 exciter (Sutter Instruments) and an Orca-R2 cooled CCD camera (Hamamatsu). The CFP fluorescence was excited at 436 nm, and the emitted light was collected at 485 nm and 535 nm using a Dual-view beam splitter (Photometrics). The images were acquired at 37°C using the Micro-Manager software (Ron Vale laboratory, University of California, San Francisco) and normalized to the initial fluorescence (F/F_0), after which the CFP/YFP ratio was calculated using ImageJ (Wayne Rasband, National Institutes of Health). Data analysis and representation were performed in Igor Pro (Wavemetrics).

Immunocytochemistry

In some experiments, the identity of the δ-cells was established by immunocytochemistry as previously described (Zhang et al., 2007, 2014b). Briefly, biocytin (0.5 mg/ml) was injected into the cells during the electrophysiology experiments via the patch pipettes. The cell type (β-, α-, or δ-cell) was established using antibodies directed against insulin, glucagon, and somatostatin, and the biocytin-loaded cells were labeled by Alexa Fluor 543–conjugated streptavidin.

Data analysis

The ΔC_m was measured once a steady-state level had been attained. Experimental data in Fig. 6, Fig. 7, Fig. 10, and Fig. 11 B were approximated using a kinetic model, which considers the transition of granules from the immediately releasable pool of granules (IRP, abbreviated *P* in the equation) and a fused state. Briefly, the pool dynamics can be described by the differential equation

$$\frac{\partial p}{\partial t} = -\alpha_0 \left(1 - e^{-\left[\frac{t}{\tau}\right]}\right)^3 p, \quad (1)$$

where t is the time after onset of depolarization, α_0 is the rate constant of exocytosis from the IRP, and τ represents the time constant for rapid granule release. Solutions to Eq. 1 were approximated from the experimental data to derive the initial values of *P*, corresponding to the maximal size of the IRP of granules. A full account of the Eq. 1 derivation has been reported previously (Barg et al., 2001).

For data in Fig. 12, time-dependent changes of electrical activity/action potential firing and $[Ca^{2+}]_i$ were detected using Clampfit, with a 20% detection threshold for both data channels and analyzed using IgorPro (Wavemetrics). Idealized traces were constructed using the peak timing of action potentials. The idealized membrane potential trace was then convolved with an exponential kernel (τ = −5 s); any $[Ca^{2+}]_i$ spikes coinciding with the resulting trace were considered as "triggered" by the membrane potential spike. The code used has been deposited to GitHub and is available upon request.

For the data in Fig. 5 and Fig. 12 D, partial area under the curve (pAUC) was estimated exactly as previously reported (Hamilton et al., 2018). Briefly, the recordings were split into 30-s intervals, and pAUC was calculated using trapezoidal integration for each interval.

All data are quoted as mean values ± SEM of the indicated number of independent experiments. Statistical significances were evaluated using Student's *t* test or ANOVA followed by a posttest (as appropriate).

Results

Glucose and tolbutamide induce electrical activity in mouse δ-cells

The following section summarizes the basic electrophysiology and somatostatin secretion of the pancreatic δ-cells. Membrane potential recordings were performed on δ-cells within intact pancreatic islets using the perforated patch whole-cell method. When exposed to 1 mM glucose, δ-cells were hyperpolarized and did not generate action potentials (APs). The resting membrane potential (V_m) averaged −72 ± 2 mV (n = 13 cells from 12 animals). Elevation of glucose to 10 mM reversibly depolarized δ-cells to a plateau potential (V_p) that averaged −55 ± 3 mV and elicited continuous electrical activity consisting of overshooting APs that peaked at (V_{peak}) +14 ± 4 mV with a firing frequency of 0.5 ± 0.1 Hz (Fig. 1 A). δ-cells express ATP-sensitive K^+-channels (K_{ATP} channels) that are of the same molecular identity (*Kcnj11* for Kir6.2, and *Abcc8* for Sur1) and comparable expression levels to those found in β-cells (Adriaenssens et al., 2016; DiGruccio et al., 2016). A saturating concentration of the K_{ATP} channel blocker tolbutamide (200 µM, half-maximal inhibition observed at 7 µM; Trube et al., 1986) exerted a glucose-like effect on δ-cell electrical activity: It depolarized the δ-cells and evoked AP firing. The APs originated from a V_p of −46 ± 3 mV (n = 13 cells from 12 animals; P < 0.01 vs. 10 mM glucose), had a V_{peak} of +5 ± 2 mV

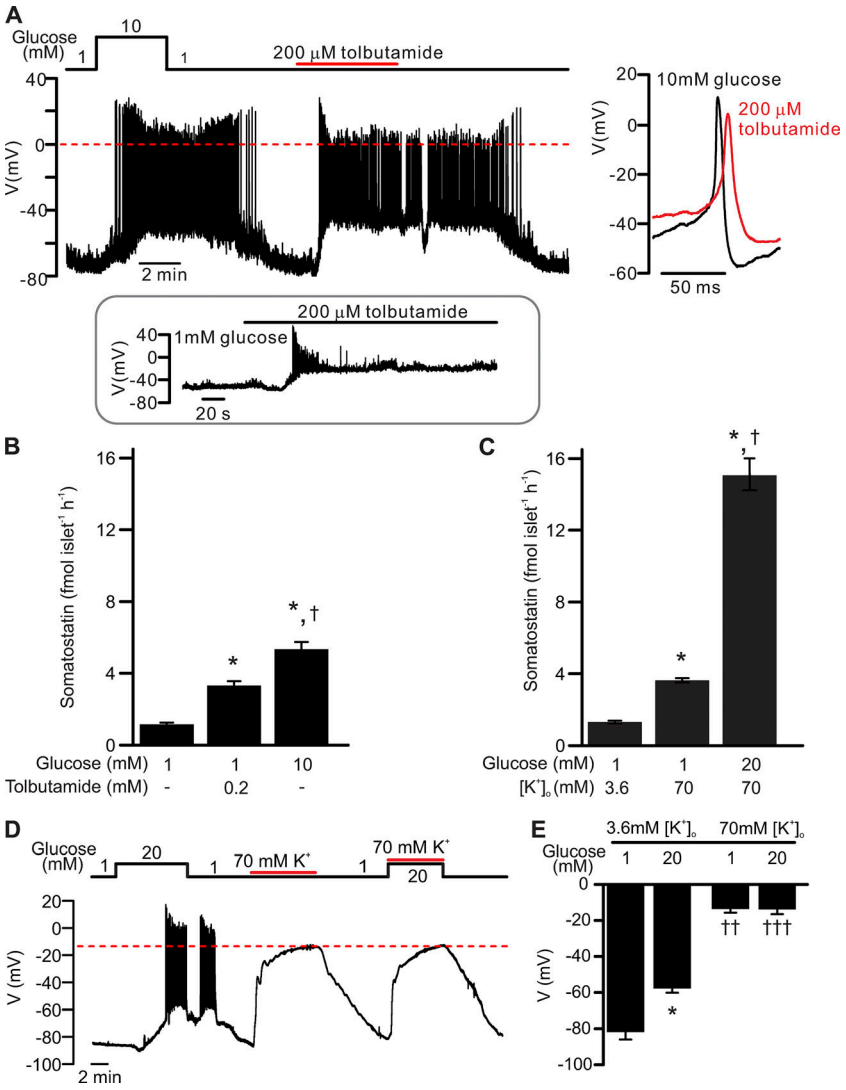

Figure 1. **δ-cell electrical activity and somatostatin secretion.** Relative roles of membrane depolarization and intracellular events in the regulation of somatostatin release–membrane depolarization in the absence of glucose is a weak stimulus for somatostatin secretion. **(A)** Electrical activity recorded from a δ-cell within an intact islet exposed to 1 mM glucose, 10 mM glucose, or 200 µM tolbutamide as indicated. The recording shown is representative of 11 out of a total 13 similar independent experiments. Zero mV is indicated by the red dashed line. Right panel shows examples of single action potentials recorded in 10 mM glucose (black) or tolbutamide (red) on an expanded time scale. Inset: Transient stimulation of electrical activity by tolbutamide in a δ-cell exposed to 1 mM glucose (seen in 2 out of 13 experiments). **(B)** Somatostatin secretion measured at 1 mM glucose (n = 20), 1 mM glucose in the presence of 0.2 mM tolbutamide (n = 10), and 10 mM glucose (n = 20) as indicated. *, P < 0.05 vs. 1 mM glucose; †, P < 0.05 vs. 0.2 mM tolbutamide. Islets are from more than three animals for each experiment, and n represents the number of independent experiments. fmol islet^{-1}h^{-1}, femtomole per islet per hour. **(C)** Somatostatin secretion measured at 3.6 mM $[K^+]_o$ with 1 mM glucose (n = 10) and at 70 mM $[K^+]_o$ with 1 mM (n = 42) or 20 mM glucose (n = 20) as indicated. *, P < 0.05 vs. 1 mM glucose at 3.6 mM $[K^+]_o$; †, P < 0.05 vs. 1 mM glucose at 70 mM $[K^+]_o$. Islets were from more than three animals for each experiment, and n represents the number of independent experiments. **(D)** Electrical activity of a δ-cell in response to physiological (3.6 mM) or supraphysiological (70 mM) $[K^+]_o$ (solid red lines) at 1 mM or 20 mM glucose (black line). Note that high $[K^+]_o$ depolarized the δ-cell to identical membrane potential in the presence of 1 mM or 20 mM glucose (dashed red line). The recording represents three independent experiments of identical conditions. **(E)** Bar graph summarizing effects of glucose and $[K^+]_o$ as indicated. *, P < 0.05 vs. 1 mM glucose at the same $[K^+]_o$; ††, P < 0.01; and †††, P < 0.001 vs. 3.6 mM $[K^+]_o$ with the same glucose concentration. All membrane potential recordings were performed using the perforated patch clamp technique. In B, C, and E, data are presented as mean ± SEM of the number of independent experiments.

(P < 0.01 vs. 10 mM glucose), and occurred at a frequency of 0.8 ± 0.1 Hz. The ∼10 mV drop in the peak voltage of the APs in response to tolbutamide is likely the consequence of the more depolarized V_p, with consequential steady-state inactivation of the voltage-gated Na^+ channels involved in AP firing (Göpel et al., 2000; Zhang et al., 2014b). In fact, the tolbutamide-induced membrane depolarization was strong enough to suppress AP firing in some cells (2 out of 13 cells; Fig. 1 A, inset), an effect reminiscent of that observed upon application of the Na^+ channel blocker tetrodotoxin (Zhang et al., 2014b).

Membrane potential–independent glucose-induced stimulation of somatostatin release

Although tolbutamide and glucose were equipotent in stimulating δ-cell electrical activity, glucose was a considerably stronger stimulus of somatostatin secretion (Fig. 1 B). Whereas tolbutamide (200 µM) stimulated somatostatin release 1.4 ± 0.2–fold above basal, glucose (10 mM) produced a 3.6 ± 0.3–fold increase.

Exocytosis in δ-cells is voltage-dependent and increases steeply between −20 and 0 mV, but there is little difference between 0 and +20 mV (Zhang et al., 2007). This suggests that the ∼10-mV reduction in AP V_{peak} (from +13 to +4 mV) cannot account for the finding that tolbutamide is a much weaker stimulus of somatostatin secretion than glucose. Thus, it is more likely that glucose augments δ-cell exocytosis by an additional intracellular signal. We next explored this aspect by measuring somatostatin in islets depolarized by a supraphysiological concentration of $[K^+]_o$ (70 mM) to bypass electrical activity.

At low glucose (1 mM), high $[K^+]_o$ stimulated somatostatin secretion 1.8 ± 0.1–fold above basal ($[K^+]_o$ = 3.6 mM). Addition of 20 mM glucose induced a further 3.2 ± 0.2–fold amplification of somatostatin release (Fig. 1 C). We ascertained that increasing glucose from 1 mM to 20 mM had no effect on δ-cell membrane potential in the presence of 70 mM $[K^+]_o$ (−14 ± 2 mV and −14 ± 3 mV, respectively; n = 3 cells from two animals; Fig. 1, D and E).

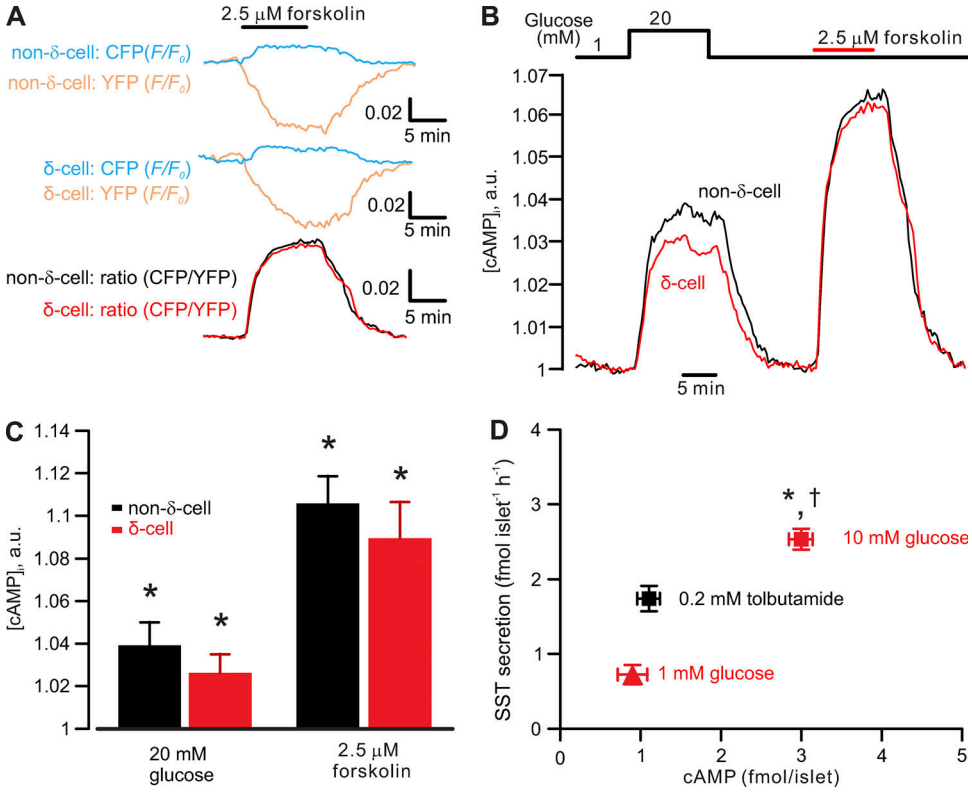

Figure 2. **Glucose- and forskolin-induced increases in cytoplasmic cAMP.** Effects of glucose on δ-cell cAMP–glucose elevates δ-cell intracellular cAMP. **(A)** Representative recordings of changes in CFP (blue traces, F/F_0) and YFP (yellow traces, F/F_0) in non–δ- (upper traces) and δ-cells (middle traces) expressing the genetically encoded cAMP sensor Epac2-camps evoked by adding 2.5 μM forskolin (indicated by the horizontal bar). The ratio of CFP and YFP (CFP/YFP, bottom traces) indicates cytoplasmic cAMP ($[cAMP]_i$) in non–δ- (black trace) or δ-cells (red trace). **(B)** Glucose- (20 mM) and forskolin-induced (2.5 μM) increases in $[cAMP]_i$ measured in non–δ- (black) and δ-cells (red) reported by Epac2-camps. **(C)** Bar graph comparing glucose- and forskolin-induced increases in $[cAMP]_i$ in δ- (n = 10 cells; expressing tdRFP) and non–δ-cells (n = 20 cells; cells not expressing tdRFP). Responses have been normalized to the level observed at 1 mM glucose. *, $P < 0.05$ vs. 1 mM glucose. **(D)** Relationship between islet cAMP content and somatostatin secretion measured in the presence of 1 mM (red triangle) and 10 mM glucose (red rectangle) or 0.2 mM tolbutamide (black rectangle; added at 1 mM glucose). *, $P < 0.05$ vs. somatostatin secretion in presence of tolbutamide; †, $P < 0.05$ vs. somatostatin secretion measured at 1 mM glucose in the absence of tolbutamide. cAMP content is higher ($P < 0.05$) in the presence of 10 mM glucose than at 1 mM glucose alone or 1 mM glucose in the presence of tolbutamide (n = 8 independent experiments from more than three mice). a.u., arbitrary unit.

Collectively, these data suggest that although membrane depolarization as such (produced by tolbutamide or 70 mM $[K^+]_o$) is capable of stimulating somatostatin secretion from δ-cells, most of the stimulation produced by glucose (>75%) is instead attributable to an amplifying effect of glucose, exerted beyond membrane depolarization and electrical activity.

Glucose increases δ-cell cytoplasmic cAMP

In α- and β-cells, glucose has been reported to elevate cytoplasmic cAMP ($[cAMP]_i$; Tian et al., 2011). We next tested whether glucose also increases $[cAMP]_i$ production in δ-cells and whether the nucleotide is responsible for transducing glucose metabolism into the amplifying signal for GISS. The following sections summarize the effects of glucose on δ-cell $[cAMP]_i$ and the effects of cAMP on GISS, δ-cell exocytosis, and $[Ca^{2+}]_i$ dynamics (Figs. 2, 3, 4, 5, 6, 7, 8, 9, 10, and 11).

First, we used a genetically encoded cAMP indicator, Epac2-camps, for time-lapse measurements of $[cAMP]_i$ in isolated single tdRFP-expressing δ-cells. Cells without tdRFP expression represent a mixture of insulin-secreting β-cells and glucagon-secreting α-cells but principally (~85%) consist of β-cells (Cabrera et al., 2006). The function of the FRET sensor was validated by measuring its response to adenylyl cyclase activator forskolin (2.5 μM) in non–δ- and δ-cells. Forskolin reversibly increased the fluorescent intensity of the FRET donor (CFP) with a concomitant reduction in YFP (acceptor) intensity. The resultant change in CFP/YFP indicates the changes in $[cAMP]_i$ (Fig. 2 A). In a series of 10 experiments, elevating glucose from 1 to 20 mM increased $[cAMP]_i$ in δ-cells to approximately the same extent as in non–δ-cells, but less than the increase produced by 2.5 μM forskolin (Fig. 2, B and C).

Next, to translate these changes in Epac2-camps signal to actual cAMP concentrations, we correlated changes in total islet cAMP content to stimulation of somatostatin secretion by measuring these two parameters in islets exposed to 1 mM glucose or 10 mM glucose (Fig. 2 D). To study the effect of electrical activity as such on cAMP content, we used 0.2 mM tolbutamide applied in the presence of 1 mM glucose.

Increasing extracellular glucose concentration from 1 to 10 mM promoted islet cAMP production >200% (from a basal 0.9

to ∼3 fmol/islet). By contrast, tolbutamide did not increase islet cAMP. Therefore, it is possible that depolarization per se is insufficient to increase cAMP in δ-cells.

Glucose amplifies somatostatin secretion by cAMP-dependent mechanisms

Because glucose increases $[cAMP]_i$, we next tested the impact of cAMP-dependent pathways in GISS from isolated islets. Glucose (10 mM) augmented somatostatin release more than fourfold. Inhibiting cAMP-dependent PKA with membrane-permeable myristolyated PKI 14–22 (abbreviated as PKI, 1 µM) or Rp-8-Br-cAMPS (100 µM) selectively inhibited GISS without affecting basal somatostatin secretion (Fig. 3, A and B). Blockade of Epac2 by ESI-05 (25 µM) exerted a similar inhibitory effect on GISS (Fig. 3 C). PKI, Rp-8-Br-cAMPS, and ESI-05 reduced the somatostatin secretion in excess of basal by 68%, 78%, and 66%, respectively. Because δ-cells express GLP-1 receptors (Richards et al., 2014), a G-protein–coupled receptor that is linked to cAMP production upon binding of GLP-1 (Thorens, 1992), we also tested whether GLP-1 stimulates GISS (Fig. 3 D). When applied at a concentration of 100 nM, GLP-1 potentiated somatostatin secretion evoked by 10 mM glucose by ∼50%. This effect was abolished by the application of 100 µM Rp-8-Br-cAMPS, which reduced somatostatin secretion below that seen in the presence of 10 mM glucose alone (probably reflecting a PKA-dependent component of GISS; see below).

The above experiments were conducted using physiological $[K^+]_o$ (3.6 mM). Therefore, part of the stimulatory effect of glucose could be exerted through an increase in δ-cell electrical activity (see Fig. 1 A). To bypass electrical activity, we next used the high $[K^+]_o$ experimental paradigm (see Fig. 1, C–E) to characterize the amplifying effect of glucose/cAMP on somatostatin secretion. Depolarization-evoked somatostatin secretion at 1 mM glucose in the absence of forskolin was not affected by 1 µM PKI, 25 µM ESI-05, or the combination of the two blockers (Fig. 4 A). Increasing glucose from 1 mM to 20 mM (Fig. 4 A), or addition of 2 µM forskolin (Fig. 4 B), induced a greater than threefold increase in depolarization-evoked somatostatin secretion. The stimulatory effect of glucose was reduced by >50% in the presence of either PKI or ESI-05 (Fig. 4 A), whereas the forskolin-stimulated somatostatin secretion was nearly completely abolished by the same blockers (Fig. 4 B). The two blockers exerted no additive effect when applied together in the presence of 20 mM glucose or forskolin, producing no further inhibition compared with either PKI or ESI-05 alone (Fig. 4, A and B).

RYR3-mediated Ca^{2+} release from intracellular Ca^{2+} stores (ER) plays a critical role for GISS (Zhang et al., 2007). We reasoned that the PKA- and Epac2-dependent amplification effects could be exerted at the level of RYR3-mediated Ca^{2+} release from the ER. This is suggested by two findings: First, depletion of intracellular Ca^{2+} stores by pretreatment with SERCA blocker thapsigargin (10 µM) abolished the augmentation of somatostatin secretion evoked by forskolin (Fig. 4 C). Second, blocking intracellular Ca^{2+} release with ryanodine (50 µM) reduced the glucose-induced amplification of depolarization-evoked somatostatin secretion by 65% (Fig. 4 D), in agreement with a similar inhibition of GISS reported previously (Zhang et al., 2007). The inhibitory effects of ryanodine and PKI or ESI-05 were not additive (Fig. 4 D), and applied in combination produced an inhibition similar to that exerted by PKI or ESI-05 alone. Finally, activating PKA and Epac2 with Sp-8-Br-cAMP (100 µM; Schwede et al., 2015a) stimulated somatostatin secretion to the same extent as 2 µM forskolin, whereas the Epac2 agonist S-223 (also known as Sp-8-BnT-2′-O-Me-cAMP; 100 µM) produced an ∼60% increase in depolarization-triggered somatostatin secretion (Fig. 4 E). The effect of S-223 was sensitive to Epac2 antagonism by ESI-05. Unexpectedly, the effect of Sp-8-Br-cAMP was also fully antagonized by ESI-05 (Fig. 4 E).

Previous work showed that δ-cells secrete somatostatin via Ca^{2+}-dependent exocytosis (Zhang et al., 2007; van der Meulen et al., 2015; Li et al., 2017). We next monitored $[Ca^{2+}]_i$ in δ-cells specifically expressing a genetically encoded Ca^{2+} indicator GCaMP3 (from SST-GCaMP3 mouse islets; see Materials and methods). Membrane depolarization by 70 mM $[K^+]_o$ increased $[Ca^{2+}]_i$ ($\Delta F/F_0$) when applied at 1 mM glucose (Fig. 5 A, *i*). However, this effect was transient, and ∼2 min after the onset of the depolarization, $[Ca^{2+}]_i$ had returned to near basal level, despite the continued presence of high $[K^+]_o$ (Fig. 5 A, *i*). The transitory nature of the high $[K^+]_o$-induced $[Ca^{2+}]_i$ elevation was not due to the membrane depolarization not being maintained (compare Fig. 1 D) but rather attributable to Ca^{2+}- and depolarization-dependent inactivation of the voltage-gated Ca^{2+} channels as previously described in β-cells (Olofsson et al., 2002).

When the same experiment was repeated in the presence of 20 mM glucose, spontaneous $[Ca^{2+}]_i$ spikes were observed before increasing $[K^+]_o$ (Fig. 5 A, *ii*). The frequency of $[Ca^{2+}]_i$ spiking was increased by high $[K^+]_o$ but, unlike what was observed at 1 mM glucose, these spikes were maintained for the entire observation period (Fig. 5 A, *ii*). Pretreating islets with thapsigargin did not abolish the spontaneous $[Ca^{2+}]_i$ spikes evoked by high glucose at 3.6 mM $[K^+]_o$, indicating that they may reflect δ-cell electrical activity and the associated Ca^{2+} entry into the δ-cells. However, in the islets pretreated with thapsigargin, elevation of $[K^+]_o$ in the presence of glucose evoked a smaller response in $[Ca^{2+}]_i$, and the $[Ca^{2+}]_i$ spikes were abolished within a few minutes (Fig. 5 A, *iii*). We quantified these data by calculating pAUC (Hamilton et al., 2018) at steady-state (during the periods indicated by gray rectangles). This analysis indicates that glucose more than doubles pAUC via a thapsigargin-sensitive mechanism (Fig. 5 B).

Glucose and forskolin amplify depolarization-triggered δ-cell exocytosis

Collectively, the data of Figs. 4 and 5 indicate that glucose and cAMP amplify somatostatin secretion by activation of intracellular ER Ca^{2+} release in depolarized δ-cells. To directly monitor the impact of glucose and forskolin on δ-cell exocytosis, we next measured exocytosis in δ-cells within the intact islet using high-resolution capacitance measurements (ΔC_m). The experiments were conducted using the perforated patch clamp configuration to maintain δ-cell metabolism.

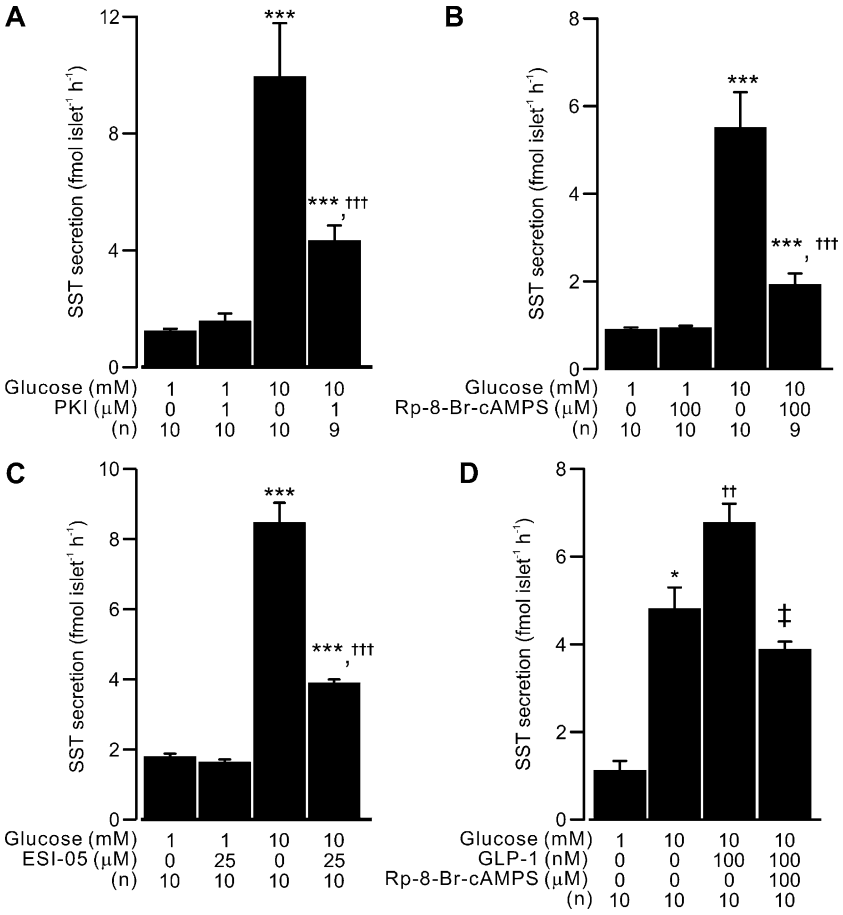

Figure 3. **Glucose-stimulated somatostatin secretion by PKA or Epac2 activation.** PKA- and Epac2-dependent pathways are involved in the regulation of somatostatin secretion. **(A)** Somatostatin secretion measured in islets exposed to 1 and 10 mM glucose under control condition or in the presence of 1 μM myristoylated PKI as indicated. **(B)** As in A, but the effect of Rp-8-Br-cAMPS (100 μM) was tested. **(C)** As in A, but the effect of 25 μM ESI-05 was tested. **(D)** As in A, but the effect of 100 nM GLP-1 on 10 mM glucose-stimulated somatostatin secretion in the presence or absence of Rp-8-Br-cAMPS (100 μM) was tested. In A–D, data are presented as mean values ± SEM for the indicated number of independent experiments (n). *, P < 0.05 and ***, P < 0.001 vs. 1 mM glucose with the same conditions; †, P < 0.05; ††, P < 0.01; and †††, P < 0.001 vs. 10 mM glucose alone (as indicated); ‡, P < 0.05 vs. 10 mM glucose in the presence of 100 nM GLP-1. $[K^+]_o$ was 3.6 mM for all the experiments, and islets were from more than three animals for each experiment.

To determine the relationship between pulse duration and somatostatin secretion, exocytosis was elicited by progressively longer depolarizations (10–500 ms) from −70 mV to 0 mV. For display purposes, only responses to 300-ms depolarizations are shown, but similar results were evoked by both shorter and longer depolarizations. Typically, the exocytotic response in δ-cells increased with pulse duration for depolarizations <300 ms but then plateaued during longer depolarizations (Zhang et al., 2007), as expected for a finite number of release-competent granules. We used this behavior to estimate the size of the IRP of granules (Eq. 1; see Materials and methods).

In the presence of 1 mM glucose, δ-cell IRP is on average 17 ± 10 fF (Fig. 6, A and B; $n = 10$). Increasing extracellular glucose to 20 mM increased δ-cell IRP approximately sevenfold to 121 ± 18 fF (Fig. 6, A and B; $n = 17$). Blocking glucokinase activity with mannoheptulose (10 mM) abolished the stimulatory effect of 20 mM glucose on exocytosis, and IRP was reduced to 29 ± 17 fF (Fig. 6, A and B; $P < 0.05$). Forskolin (2 μM) mimicked the effect of glucose, but the effect was slightly weaker (not statistically significant), and IRP averaged 77 ± 14 fF ($n = 5$, $P < 0.05$ vs. 1 mM glucose group; Fig. 6, A and B). The IRP corresponds to the number of granules that can be released with minimal delay (i.e., during action potential firing). Our biophysical estimates of IRP can be converted to the number of somatostatin-containing secretory granules using a conversion factor of 1 fF/granule (estimated from electron microscopy; (Göpel et al., 2004). Thus, IRP corresponds to ∼15 granules at 1 mM glucose and increases to >100 granules in the presence of high glucose.

We considered the possibility that glucose stimulates exocytosis and CICR by promoting intracellular Ca^{2+} storage in the ER. This would be consistent with the strong effects of thapsigargin on glucose-induced $[Ca^{2+}]_i$ in δ-cells (see Fig. 5 A, iii; and Fig. 5 B) and somatostatin secretion (Zhang et al., 2007). We addressed this question by photoreleasing $InsP_3$ from its caged precursor (50 μM) in δ-cells preincubated at 1 or 20 mM glucose (>1 h). This is based on our previous observation that δ-cell $InsP_3$ receptors and RYR-dependent ER Ca^{2+} stores communicate (Zhang et al., 2007). In δ-cells exposed to 20 mM glucose, $InsP_3$ triggered a Ca^{2+} transient (indicated by Fluo-4 fluorescence, ΔF) that was threefold greater than that seen in δ-cells exposed to 1 mM glucose (Fig. 6, C and D). This glucose effect on $InsP_3$-triggered $[Ca^{2+}]_i$ correlated with a threefold stimulation of the initial rate of exocytosis (Fig. 6, E and F; expressed as $\delta C_m/\delta t$; $P < 0.05$ vs. 1 mM glucose), suggesting that glucose promotes sequestration of Ca^{2+} into the ER. In addition, these data provide direct evidence that intracellular Ca^{2+} release is sufficient to elicit exocytosis in δ-cells.

cAMP augments depolarization-evoked exocytosis and increases $[Ca^{2+}]_i$ in δ-cells

CICR plays a critical role in somatostatin secretion from δ-cells (Zhang et al., 2007; Li et al., 2017). We next examined the impact of intracellular cAMP on the depolarization-evoked $[Ca^{2+}]_i$ transients and cellular exocytosis in δ-cells (Fig. 7). In this series of experiments, we used standard whole-cell configuration,

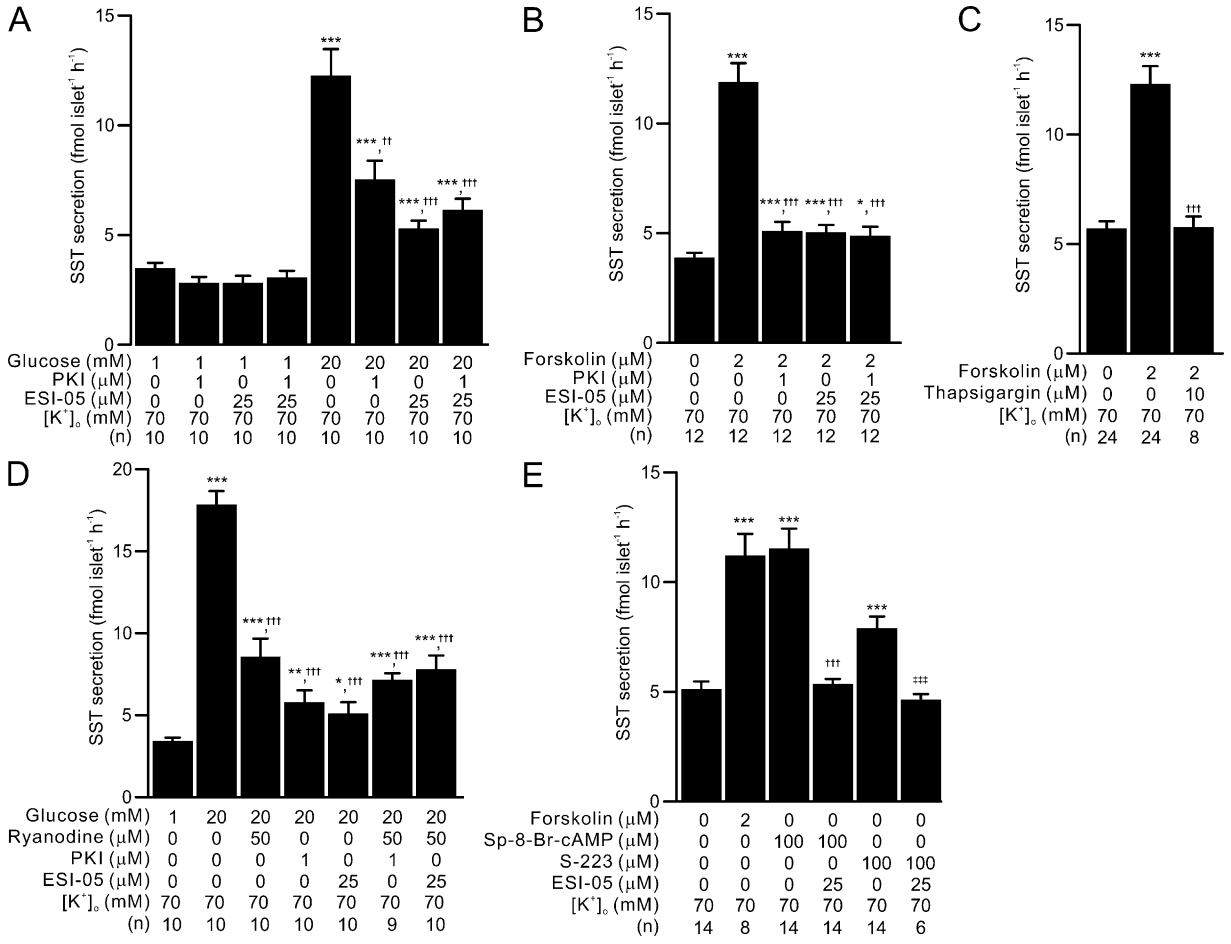

Figure 4. **PKA- and Epac2-dependent effects of glucose and forskolin on depolarization-induced somatostatin secretion by ER Ca^{2+} release.** PKA- and Epac2-dependent intracellular Ca^{2+} release is involved in somatostatin secretion in depolarized δ-cells—an effect that is independent of membrane depolarization. **(A)** Somatostatin secretion in response to 1 mM and 20 mM glucose in islets depolarized with 70 mM $[K^+]_o$ under control conditions and in the presence of PKI (1 μM), ESI-05 (25 μM), or both blockers, as indicated. ***, P < 0.001 vs. 1 mM glucose under same condition; ††, P < 0.01 and †††, P < 0.001 vs. 20 mM glucose alone. **(B)** Somatostatin secretion measured in the absence and presence of 2 μM forskolin (at 1 mM glucose) in islets depolarized with 70 mM $[K^+]_o$. Effect of PKI (1 μM), ESI-05 (25 μM), or simultaneous application of both blockers on forskolin-stimulated somatostatin secretion was tested. *, P < 0.05 and ***, P < 0.001 vs. somatostatin secretion under control condition; †††, P < 0.001 vs. somatostatin in the presence of 2 μM forskolin alone. **(C)** As in B but testing the effect of preincubation with thapsigargin (10 μM, 1 h) on 2 μM forskolin-stimulated somatostatin secretion (triggered by 70 mM $[K^+]_o$). ***, P < 0.001 vs. somatostatin secretion under the control condition; †††, P < 0.001 vs. somatostatin secretion in the presence of 2 μM forskolin alone. **(D)** Somatostatin secretion in response to 1 mM and 20 mM glucose in islets depolarized with 70 mM $[K^+]_o$ under control condition and in the presence of ryanodine, PKI or ESI-05 as indicated. *, P < 0.05; **, P < 0.01; and ***, P < 0.001 vs. 1 mM glucose alone; †††, P < 0.001 vs. 20 mM glucose alone. **(E)** 70 mM $[K^+]_o$-triggered somatostatin secretion measured in the absence and presence of forskolin (2 μM), Sp-8-Br-cAMP (100 μM), or Epac2 agonist (S-223, 100 μM). ESI-05 (25 μM) was applied in the presence of Sp-8-Br-cAMP or S-223 to test the specificity of the agonists. ***, P < 0.001 vs. somatostatin secretion under the control condition; †††, P < 0.001 vs. somatostatin secretion in the presence of 100 μM Sp-8-Br-cAMP alone; and ‡‡‡, P < 0.001 vs. somatostatin secretion in the presence of 100 μM S-223 alone. In A–E, data are presented as mean values ± SEM for the indicated numbers of independent experiments (n). Islets from more than three animals were used for each experiment.

which allows direct intracellular application of a Ca^{2+} indicator (indo-1) and cAMP through patch clamp electrodes. The δ-cells were stimulated by a series of progressively longer depolarizations (for 10–500 ms, from −70 mV to 0 mV), applied with an interval of 20 s.

We determined the impact of cAMP on basal $[Ca^{2+}]_i$, peak $[Ca^{2+}]_i$, and duration of the spike (Fig. 7, B and D; and Table 2) and correlated the changes to exocytotic capacity (Fig. 7, A and C, measured as IRP). cAMP effects on exocytosis and basal $[Ca^{2+}]_i$ were undetectable at 1 μM, half-maximal at 3 μM, and maximal at ≥10 μM (Fig. 7, A–D). At high $[cAMP]_i$ (≥10 μM), IRP increased more than fourfold, and basal $[Ca^{2+}]_i$ increased from ∼50 nM to ∼200 nM (Fig. 7, C and D). Increasing $[cAMP]_i$ from 0 to 100 μM also increased peak $[Ca^{2+}]_i$ by ∼100% and extended the duration of the spikes (half width) by >50% (Table 2). This effect is not due to changes in Ca^{2+} currents induced by cAMP. Ca^{2+} current measured in response to a depolarization (from −70 mV to 0 mV) in the presence of 100 μM cAMP was −70 ± 7 pA (n = 7), which was marginally less than, though not statistically different from, that recorded in the absence of cAMP (−80 ± 7 pA; n = 12). Pretreatment with thapsigargin abolished the effect of 100 μM cAMP on both exocytosis and $[Ca^{2+}]_i$ (red traces in Fig. 7,

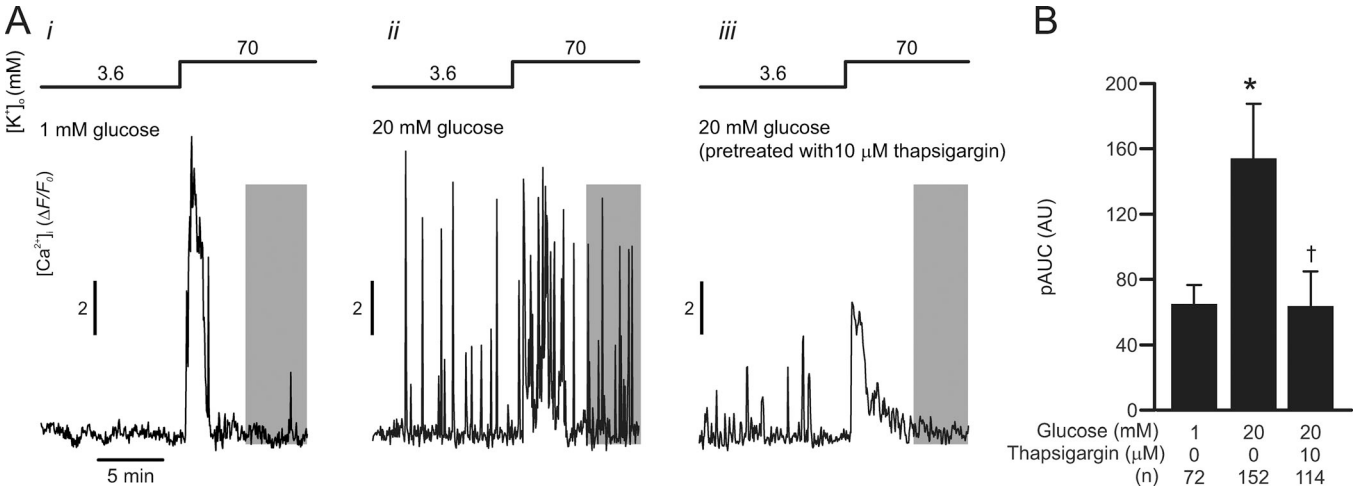

Figure 5. **Glucose-stimulated $[Ca^{2+}]_i$ oscillations in high $[K^+]_o$-depolarized δ-cells.** δ-cell Ca^{2+} release from the ER is stimulated by glucose. **(A)** Examples of δ-cell $[Ca^{2+}]_i$ ($\Delta F/F_0$) recorded from SST-GCaMP3 islets in response to increasing $[K^+]_o$ from 3.6 mM to 70 mM as indicated. Experiments were conducted with extracellular media containing (*i*) 1 mM glucose and (*ii*) 20 mM glucose in islets cultured in control RPMI medium; and (*iii*) 20 mM glucose in islets incubated with RPMI medium containing 10 μM thapsigargin (>1 h). **(B)** Summary of 70 mM $[K^+]_o$-triggered δ-cell $[Ca^{2+}]_i$ (pAUC) at steady-state (gray areas in A) under the experimental conditions indicated below. *, $P < 0.05$ vs. 1 mM glucose and †, $P < 0.05$ vs. 20 mM glucose without pretreatment of thapsigargin. Data are presented as mean values ± SEM of the indicated numbers of GCaMP3-expressing δ-cells (n) from two or three mice for each experimental condition. AU, arbitrary unit.

A and B; red rectangles in Fig. 7, C and D; and Table 2). We note that the thapsigargin effect on exocytosis observed here appears slightly stronger than that in our previous report (Zhang et al., 2007), a difference that may reflect different extracellular solutions used in this and the previous study (1 mM and 20 mM glucose, respectively).

Consistent with our previous report (Zhang et al., 2007), the depolarization-triggered capacitance increases extended beyond the duration of depolarizations when the experiments were performed in the presence of cAMP (slow component of exocytosis, indicated by arrows in Fig. 7 A). This component of exocytosis was abolished by pretreatment with thapsigargin and absent when $[cAMP]_i$ was ≤1 μM. The slow component of exocytosis correlated with a prolongation of the depolarization-evoked $[Ca^{2+}]_i$ increases in the presence of cAMP, which was sensitive to thapsigargin (Fig. 7 B). In the absence of cAMP, the $[Ca^{2+}]_i$ peaked within <200 ms after the end of the depolarization, which was followed by a smooth decay toward the baseline (Fig. 7 B). By contrast, in the presence of 100 μM cAMP, the δ-cell $[Ca^{2+}]_i$ continued to increase and did not decline until >500 ms after the end of the depolarization. This correlated with an approximately threefold increase in $[Ca^{2+}]_i$ transients area under the curve (AUC) compared with the control ($P < 0.05$; Fig. 7 D, inset). These effects of cAMP were prevented by pretreatment with thapsigargin (Fig. 7 B), and the $[Ca^{2+}]_i$ transients AUC was reduced to a level close to the control.

To further confirm the intracellular nature of the effect of cAMP on δ-cell exocytosis and CICR, we measured depolarization-triggered $[Ca^{2+}]_i$ transients and exocytosis in SST-GCaMP3 δ-cells before and after the application of forskolin, using the perforated patch configuration. In a series of five experiments, exposure to 10 μM forskolin for 5 min significantly augmented $[Ca^{2+}]_i$ transients triggered by 300-ms depolarizations from −70 to 0 mV (Fig. 7 E; $P < 0.05$). The increase in $[Ca^{2+}]_i$ transient magnitude correlated with an approximately fourfold increase in δ-cell exocytosis (from 9 ± 2 fF to 38 ± 10 fF; $n = 5$; $P < 0.05$). Interestingly, the adenylyl cyclase activator also induced spontaneous $[Ca^{2+}]_i$ spikes (arrows in Fig. 7 E, inset) in δ-cells voltage-clamped at −70 mV (to prevent opening of voltage-gated Ca^{2+} channels). Together, the data in Fig. 7 demonstrate that increases in intracellular cAMP enhance depolarization-evoked CICR and exocytosis in δ-cells.

cAMP induces spontaneous $[Ca^{2+}]_i$ spikes in δ-cells

Consistent with the data in Fig. 7 E, intracellular application of cAMP also induced spontaneous Ca^{2+} spikes in δ-cells (indicated by arrows in Fig. 8, C and D). In cells infused with 10–100 μM cAMP, 67% of the δ-cells (six of nine cells from eight animals) displayed Ca^{2+} transients even when voltage-clamped at −70 mV but were seen in ∼30% of the δ-cells (4 of 14 cells) dialyzed with a solution containing ≤1 μM cAMP (Fig. 8, A and B). Variable in duration, the magnitude of these spikes was comparable to the increase in $[Ca^{2+}]_i$ produced by a 10-ms depolarization from −70 to 0 mV (Fig. 8, C and D). The cAMP-induced spontaneous $[Ca^{2+}]_i$ spikes were abolished by pretreating islets with 10 μM thapsigargin (Fig. 8 E). We point out that these $[Ca^{2+}]_i$ spikes are not apparent in the traces in Fig. 7 B, in which the data for several cells have been averaged. Depletion of ER Ca^{2+} with thapsigargin was not associated with any detectable increase in the holding current at −70 mV (not shown). Thus, store-operated Ca^{2+} influx plays little or no role in the δ-cells under the experimental conditions pertaining to these experiments.

The spontaneous δ-cell $[Ca^{2+}]_i$ spikes in the presence of cAMP may contribute to the cAMP-induced increase in δ-cell basal $[Ca^{2+}]_i$. Next we tested whether changes in basal $[Ca^{2+}]_i$ alone would affect δ-cell exocytosis. We did this by clamping $[Ca^{2+}]_i$

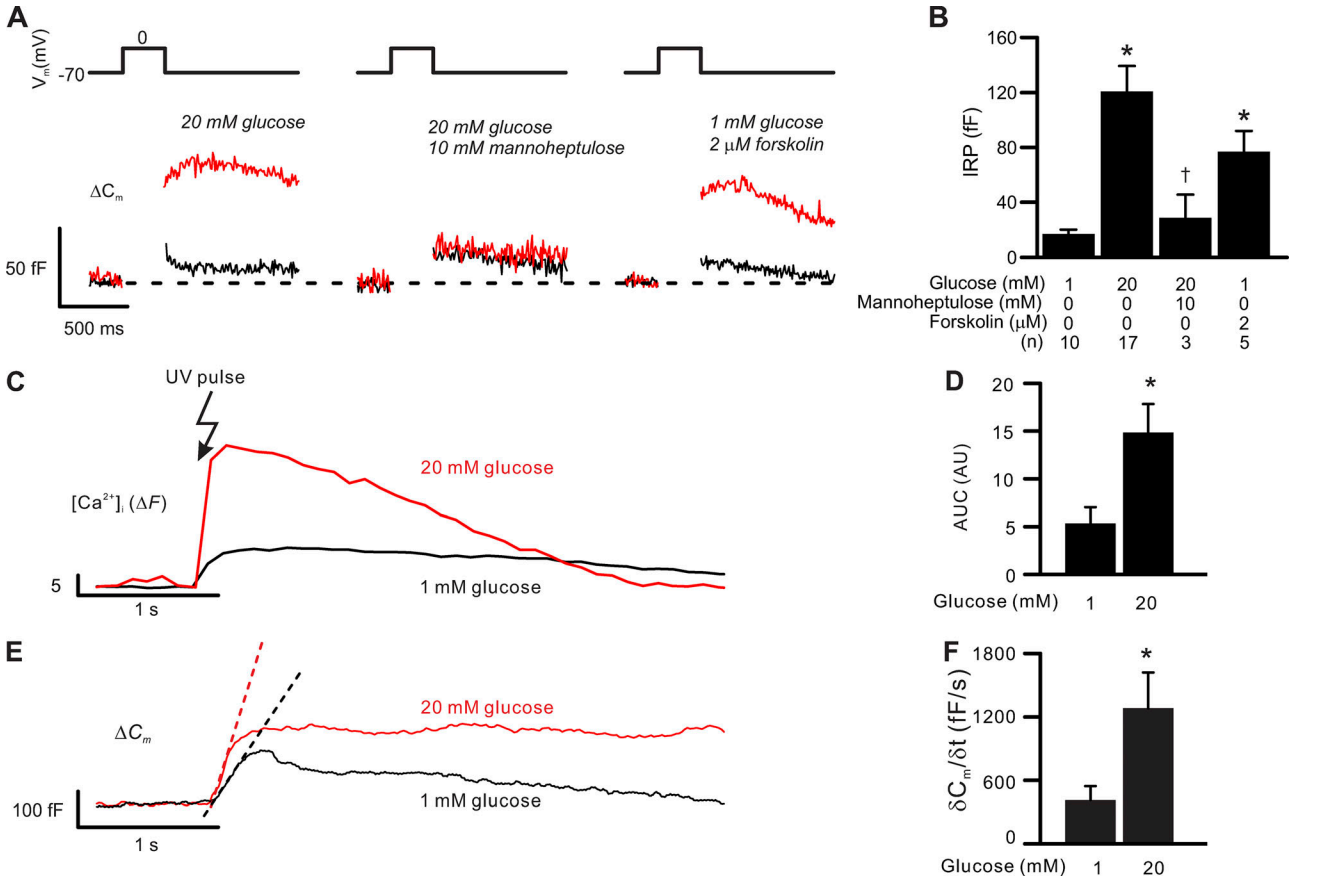

Figure 6. **Glucose metabolism stimulates exocytosis and ER Ca^{2+} uptake in δ-cells.** Exocytosis and ER Ca^{2+} uptake in δ-cells are stimulated by glucose metabolism or forskolin. **(A)** Exocytosis (measured as increases in membrane capacitance, bottom traces, ΔC_m) triggered by 300-ms depolarizations from −70 mV to 0 mV (top) in δ-cells exposed to indicated experimental conditions (red). The black traces show the exocytotic responses triggered by identical pulses in the same cells exposed to 1 mM glucose alone. The experiments were conducted using perforated patch whole-cell configuration. **(B)** Summary of exocytotic response (IRP) in δ-cells perfused with extracellular solutions containing glucose (1 mM and 20 mM), forskolin (2 μM), and 10 mM mannoheptulose in the presence of 20 mM glucose. *, P < 0.05 vs. 1 mM glucose and †, P < 0.05 vs. 20 mM glucose alone. Data are mean values ± SEM of indicated number of independent experiments (n) from 2–14 animals. **(C)** Increase in $[Ca^{2+}]_i$ (ΔF) triggered by photorelease of caged $InsP_3$ precursor in δ-cells preincubated at 1 mM (black) or 20 mM glucose (red) for >1 h. Photoliberation was effected by a flash of UV light as indicated. Traces are representative responses of similar independent experiments (n = 4 for 1 mM and 20 mM glucose). **(D)** Summary of data in C. *, P < 0.05 vs. 1 mM glucose. Data are mean values ± SEM of four independent experiments from two to four animals for each experimental condition. **(E)** As in C but shows the δ-cell exocytosis (ΔC_m) in response to photoliberation of $InsP_3$. Pre-incubation glucose concentrations are as indicated. The dotted lines indicate the slope of initial capacitance increase. **(F)** Summary of the initial exocytotic rate ($\delta C_m/\delta t$) following photorelease of $InsP_3$ in δ-cells preincubated at 1 mM or 20 mM glucose for >1 h. *, P < 0.05 vs. 1 mM glucose. The exocytotic rate was calculated by differentiating the rising slope of capacitance increase in response to increases in cytosolic $InsP_3$. Data are mean values ± SEM of four independent experiments from two to four animals for each experimental condition. In C–F, experiments were conducted using standard whole-cell technique without addition of cAMP in the intracellular solution.

through infusion via the patch pipettes of an intracellular solution containing 103 nM or 240 nM free Ca^{2+} but no cAMP for 5 min preceding a depolarization (from −70 mV to 0 mV for 500 ms) that triggered exocytosis. This moderate increase in basal $[Ca^{2+}]_i$ stimulated depolarization-evoked exocytosis by 80% (Fig. 9, A and B).

Does an increase in basal $[Ca^{2+}]_i$ enhance δ-cell CICR? We tested this by measuring the $[Ca^{2+}]_i$ transients triggered by 500-ms depolarizations (from −70 to 0 mV) before and after a prolonged (2 min) low-amplitude depolarization (from −70 to −40 mV). This set of experiments was conducted in δ-cells in islets from SST-GCaMP3 mice exposed to 1 mM glucose using the perforated patch clamp technique. As shown in Fig. 9 C, the moderate depolarization produced a moderate but sustained increase in $[Ca^{2+}]_i$, but the second pulse to 0 mV did not trigger larger $[Ca^{2+}]_i$ increases than the first pulse (Fig. 9, C and D). Therefore, at low glucose, it is not apparent that an increase in basal $[Ca^{2+}]_i$ per se is sufficient to enhance δ-cell CICR.

cAMP-dependent δ-cell exocytosis relies on CICR

The observed cAMP effect can be mediated by PKA- or Epac2-dependent pathways, and blocking the two cAMP effectors strongly inhibited GISS (see Figs. 3 and 4). We next analyzed the contribution of PKA- and Epac2-mediated mechanisms in the control of δ-cell exocytosis and $[Ca^{2+}]_i$. The Epac2 agonist 2′-O-Me-cAMP (100 μM) or cAMP (100 μM) was infused into δ-cells via the patch pipettes during standard whole-cell measurements, in the absence or presence of inhibitors of PKA (PKI; 1 μM) or Epac2 (ESI-05; 25 μM).

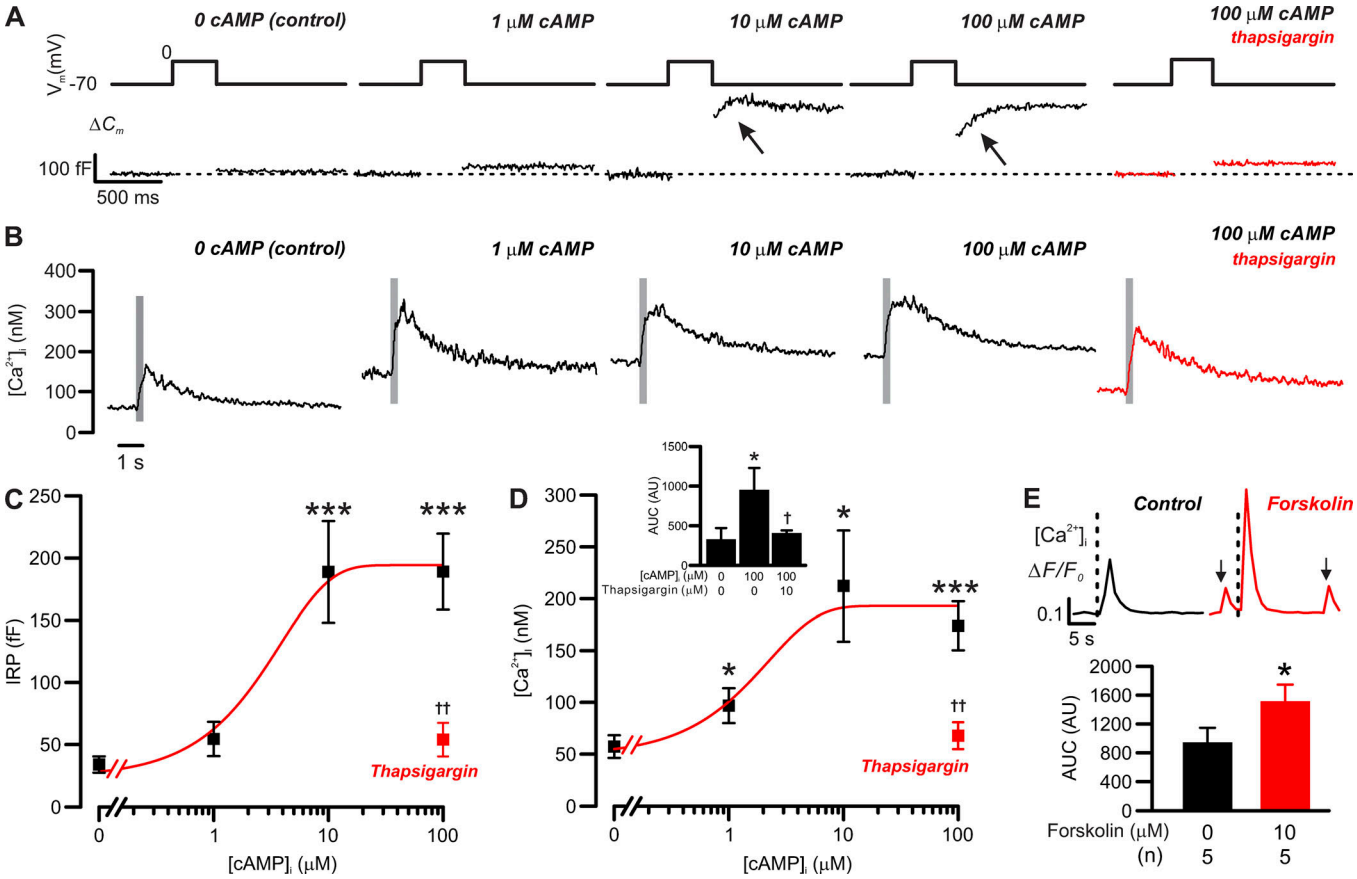

Figure 7. **cAMP-dependent increases in exocytosis and basal $[Ca^{2+}]_i$ in δ-cells.** Correlation between $[cAMP]_i$ and δ-cell $[Ca^{2+}]_i$/exocytosis. **(A)** Exocytosis (ΔC_m; bottom) evoked by 300-ms depolarizations from −70 mV to 0 mV (top) in δ-cells dialyzed with cAMP at the indicated concentrations. Red trace shows the response with 100 μM cAMP following treatment with 10 μM thapsigargin. **(B)** As in A but showing the changes in cytoplasmic $[Ca^{2+}]_i$ (on a compressed timescale). Gray areas mark the periods of 300-ms membrane depolarizations from −70 mV to 0 mV. Note that $[Ca^{2+}]_i$ traces are averaged responses of experiments of the same conditions. **(C)** Summary of cAMP dose-dependent effect on δ-cell immediate releasable pool (IRP; n = 14 independent experiments for control, 6 for 1 μM cAMP, 5 for 10 μM cAMP, 6 for 100 μM cAMP, and 4 for 100 μM cAMP pretreated with 10 μM thapsigargin; ***, P < 0.001 vs. control). Red rectangle indicates the response with 100 μM cAMP following pretreatment with 10 μM thapsigargin for > 1 h. ††, P < 0.01 vs. 100 μM cAMP alone. **(D)** As in C but summarizes the response of basal $[Ca^{2+}]_i$ (n = 9 independent experiments for control, 5 for 1 μM cAMP, 3 for 10 μM cAMP, 5 for 100 μM cAMP, and 4 for 100 μM cAMP pretreated with 10 μM thapsigargin for >1 h; *, P < 0.05 and ***, P < 0.001 vs. control). Red rectangle indicates the response with 100 μM cAMP following pretreatment with 10 μM thapsigargin. ††, P < 0.01 vs. 100 μM cAMP alone. In C and D, data are presented as mean values ± SEM for the number of independent experiments (n) from two to eight animals. Inset summarizes the AUC of depolarization-triggered $[Ca^{2+}]_i$ transients in δ-cells infused with cAMP of the indicated concentrations. Red bar shows the response in thapsigargin-pretreated δ-cells infused with 100 μM cAMP. Data are mean values ± SEM for the number of independent experiments (n) from two to eight animals. *, P < 0.05 vs. control and †, P < 0.05 vs. 100 μM cAMP without thapsigargin pretreatment. **(E)** Bar graph shows the average AUC of $[Ca^{2+}]_i$ transients triggered by 300-ms depolarizations before (black) and after application of 10 μM forskolin (red). Data are presented as mean values ± SEM of indicated numbers of independent experiments (n) from two animals. *, P < 0.05 vs. control (before forskolin application). Inset shows examples of 300-ms depolarizations (from −70 to 0 mV) triggered δ-cell $[Ca^{2+}]_i$ transients, recorded in the same cells, before (control, black) and after the application of forskolin (forskolin, red) for 5 min. Onset of the depolarizing pulses is indicated by vertical dotted lines. Arrows indicate spontaneous Ca^{2+} spikes that were observed in the absence of membrane depolarization. The traces are aligned to the same baseline to facilitate the comparison of $[Ca^{2+}]_i$ transient kinetics. Measurements in A–D were conducted using the standard whole-cell technique. Experiments in E were conducted using perforated patch clamp technique.

The stimulatory effect of 100 μM cAMP on δ-cell exocytosis (blue traces in Fig. 10 A and blue dotted line in Fig. 10 C) was reduced by 70% in the presence of PKI or ESI-05. Whereas ESI-05 counteracted the effect of cAMP on basal $[Ca^{2+}]_i$ to the same extent as thapsigargin (compare Fig. 7, C and D), PKI had no effect (Fig. 10, B and D; and Table 2). Selective activation of Epac2 by 100 μM 2′-O-Me-cAMP had similar effects on $[Ca^{2+}]_i$ as cAMP in the presence of PKI: It increased basal $[Ca^{2+}]_i$ and broadened the Ca^{2+} transients but did not affect peak $[Ca^{2+}]_i$ (Fig. 10, B and D; and Table 2). In addition, whereas the spontaneous cAMP-induced $[Ca^{2+}]_i$ spikes were abolished by ESI-05, they persisted in δ-cells infused with 2′-O-Me-cAMP or cAMP with addition of PKI (Fig. 10, E–G). In the presence of PKI, the depolarization-evoked $[Ca^{2+}]_i$ transients were sometimes distinctly biphasic with a secondary increase (red arrows in Fig. 10 F) occurring with a delay of ≈2 s (2 out of 10 cells). This was echoed by the similar observation (red arrows in Fig. 10 E) in 67% of the δ-cells (four out of six cells) infused with the Epac2 agonist 2′-O-Me-cAMP (100 μM). It may be speculated that some basal PKA activity is required for efficient coupling between Ca^{2+} entry and Epac2/RYR3-dependent activation of CICR.

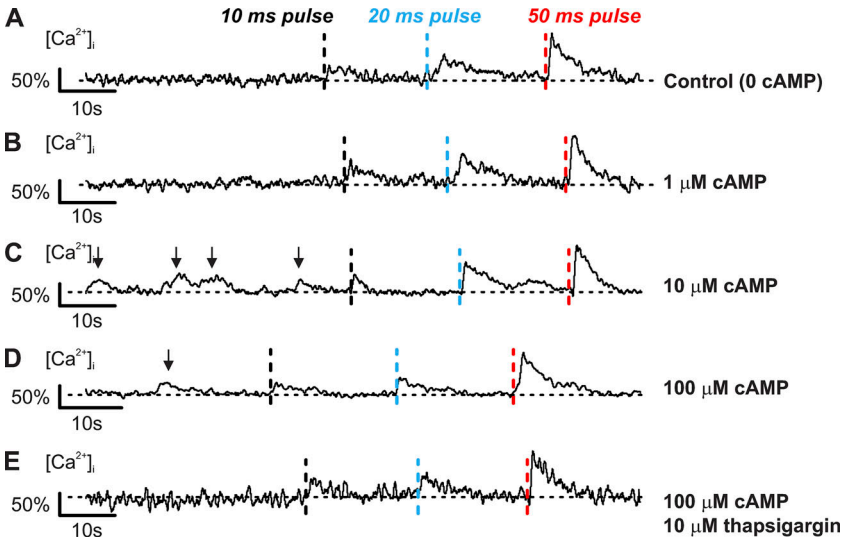

Figure 8. **Spontaneous cAMP-dependent $[Ca^{2+}]_i$ transients in voltage-clamped δ-cells.** Spontaneous thapsigargin-sensitive $[Ca^{2+}]_i$ spikes evoked by cAMP. **(A–D)** $[Ca^{2+}]_i$ recorded in δ-cells held at −70 mV and infused with cAMP (concentrations as indicated) using the standard whole-cell technique. Three consecutive depolarizations from −70 mV to 0 mV with increasing durations were applied: 10 ms (black dotted lines), 20 ms (blue dotted lines), and 50 ms (red dotted lines). Depolarizations were applied with >20-s intervals. **(E)** As in D but after preincubation with 10 µM thapsigargin for >1 h. Responses are normalized to the $[Ca^{2+}]_i$ increase evoked by a 50-ms depolarization to 0 mV. Recordings are representative of six (A), five (B), three (C), five (D), and four (E) independent experiments from two to five animals. Arrows above traces indicate the spontaneous $[Ca^{2+}]_i$ spikes.

The effects of ESI-05 on cAMP-induced stimulation of exocytosis and basal $[Ca^{2+}]_i$ were echoed by the results of genetic ablation of *Epac2*. In δ-cells from *Epac2* knockout mice (*Epac2*$^{-/-}$), basal $[Ca^{2+}]_i$ was not increased by intracellular application of 100 µM cAMP, unlike what was observed in wild-type (*Epac2*$^{+/+}$) δ-cells (Fig. 11 A). The effects of ablating *Epac2* on $[Ca^{2+}]_i$ were paralleled by reduced cAMP-induced augmentation of depolarization-evoked exocytosis compared with *Epac2*$^{+/+}$ δ-cells (Fig. 11 B). These changes correlate with reduced GISS (Fig. 11, C and D). Whereas 200 µM tolbutamide produced a similar stimulation of somatostatin secretion from both *Epac2*$^{+/+}$ and *Epac2*$^{-/-}$ islets, GISS from *Epac2*$^{-/-}$ islets was ∼20% lower than that seen in the *Epac2*$^{+/+}$ islets ($P < 0.05$). Inhibition of PKA with Rp-8-Br-cAMPS abolished GISS in *Epac2*$^{-/-}$ islets and reduced secretion to a level below that evoked by tolbutamide

Table 2. **Kinetics of depolarization-triggered $[Ca^{2+}]_i$ transients in δ-cells**

$[cAMP]_i$ (µM)	Treatment	$[Ca^{2+}]_{peak}$ (nM)	Half width (ms)	*n*
0	n/a	185 ± 60	226 ± 30	8
1	n/a	347 ± 88	207 ± 17	5
10	n/a	326 ± 35	282 ± 17	3
100	n/a	353 ± 56[a]	347 ± 36[a]	5
0	100 µM 2′-O-Me-cAMP	232 ± 34[b]	465 ± 121[a]	7
100	10 µM thapsigargin	286 ± 45	301 ± 12	4
100	1 µM myr-PKI	347 ± 53[a]	558 ± 106[a]	6
100	25 µM ESI-05	225 ± 39	291 ± 34	4

Peak ($[Ca^{2+}]_{peak}$) and duration (half width) of $[Ca^{2+}]_i$ transients triggered by 300-ms depolarizations from −70 mV to 0 mV in δ-cells infused with intracellular solutions containing cAMP with concentrations indicated. The Treatment column lists the compounds that were infused into δ-cells at the indicated concentrations in the presence of 100 µM cAMP (with the exception of thapsigargin, which was applied extracellularly during the pretreatment of the islets). Data are presented as mean values ± SEM of indicated number of independent experiments (*n*) from two to eight animals. All the measurements were made using standard whole-cell technique. n/a, not applicable.

[a]$P < 0.05$ vs. control (no addition of cAMP).

[b]$P < 0.05$ vs. 100 µM cAMP alone.

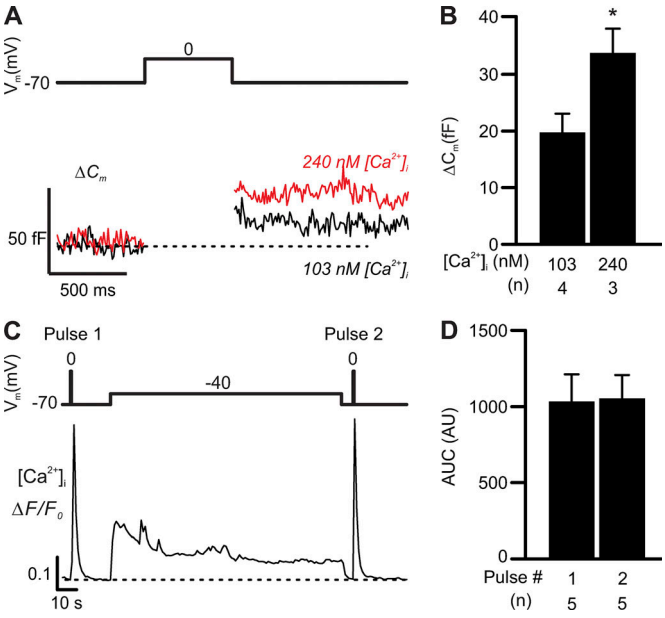

Figure 9. **Elevation of basal $[Ca^{2+}]_i$ potentiates δ-cell exocytosis but not CICR. (A)** Moderate elevation of $[Ca^{2+}]_i$ potentiates exocytosis but not CICR. Exocytosis (ΔC_m, lower) triggered by 500-ms depolarizations from −70 to 0 mV (V_m, top) in δ-cells infused with 103 nM or 240 nM free Ca^{2+} through patch pipettes. **(B)** Bar graph summarizing the effects of indicated number of independent experiments (n) from two or three animals for each condition. *, $P < 0.05$ vs. 103 nM $[Ca^{2+}]_i$. **(C)** δ-cell $[Ca^{2+}]_i$ transients (lower, $\Delta F/F_0$) triggered by 500-ms depolarizations (from −70 to 0 mV) before (pulse 1) and after (pulse 2) a 2-min depolarization from −70 to −40 mV (top). The average AUC of $[Ca^{2+}]_i$ transients triggered by pulses 1 and 2 of indicated number of independent experiments (n, from three animals) are summarized in D. Experiments in A and B were conducted using standard whole-cell technique. Data in B and D are presented as mean ± SEM of the numbers of independent experiments as indicated. Experiments in C and D were conducted using perforated patch clamp technique.

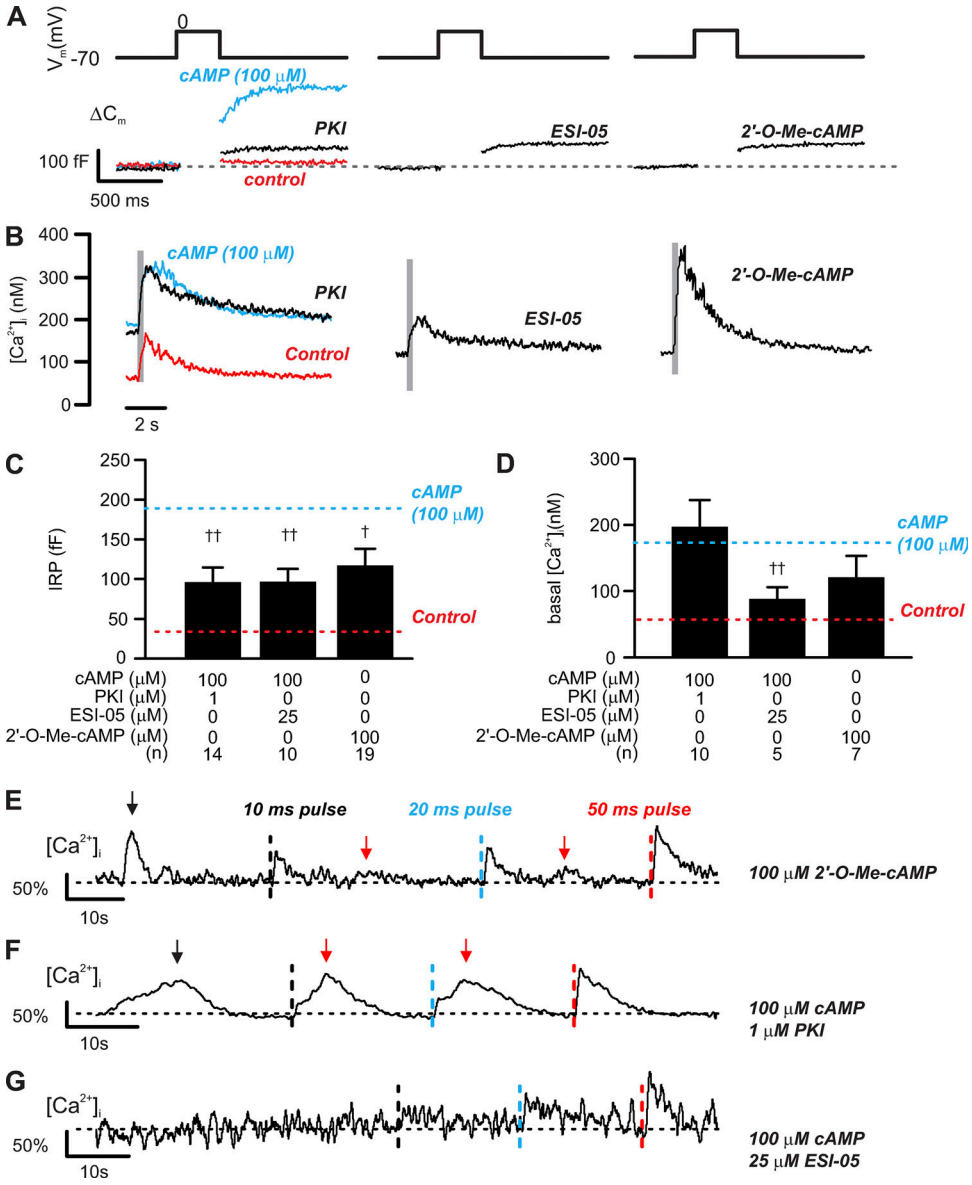

Figure 10. **PKA-dependent and -independent effect of cAMP on δ-cell exocytosis.** PKA and Epac2 differentially regulate depolarization-evoked exocytosis and $[Ca^{2+}]_i$ increase. **(A)** Exocytosis (ΔC_m; bottom) evoked by 300-ms depolarizations from −70 mV to 0 mV (top) in δ-cells dialyzed with cAMP (100 μM) together with inhibitors of PKA (PKI, 1 μM), Epac2 (ESI-05, 25 μM), or Epac2 agonist (2′-O-Me-cAMP, 100 μM) alone as indicated. **(B)** The averaged $[Ca^{2+}]_i$ responses of experiments of the same conditions. In A and B, red and blue traces represent responses seen in control (without cAMP) and 100 μM cAMP, respectively, and are inserted here for comparison. Note that different time scales are used for the electrophysiological measurements and recordings of $[Ca^{2+}]_i$. Gray rectangles correspond to the 300-ms depolarizations from −70 to 0 mV. **(C and D)** IRP and basal $[Ca^{2+}]_i$ determined under the indicated experimental conditions. Data are mean values ± SEM for indicated number of independent experiments (n) from 4–15 animals for each experimental condition. †, $P < 0.05$ and ††, $P < 0.01$ vs. 100 μM cAMP. Red and blue dotted lines indicate responses seen in control (without cAMP) and 100 μM cAMP, respectively. **(E)** $[Ca^{2+}]_i$ recorded in δ-cells held at −70 mV and infused with Epac2 agonist (2′-O-Me-cAMP, 100 μM). Three consecutive depolarizations from −70 mV to 0 mV were applied with increasing durations: 10 ms (black dotted lines), 20 ms (blue dotted lines), and 50 ms (red dotted lines). Depolarizations were applied with >20-s intervals. **(F and G)** As in E, but cells were infused with solutions containing 100 μM cAMP with inclusion of PKI (1 μM; F) or ESI-05 (25 μM; G). Responses were normalized to the 50-ms depolarization-triggered $[Ca^{2+}]_i$ transients. Recordings are representative of 7 (E), 10 (F), and 5 (G) independent experiments from four to eight animals. Black arrows above the traces indicate the spontaneous $[Ca^{2+}]_i$ spikes before depolarization, and red arrows indicate the second increase in $[Ca^{2+}]_i$ following depolarizations. All measurements were made using the standard whole-cell technique.

($P < 0.05$). By contrast, 60% of GISS was resistant to the PKA inhibitor in *Epac2*$^{+/+}$ islets ($P < 0.05$; Fig. 11, C and D). This suggests that Rp-8-Br-cAMPS specifically inhibits PKA and does not exert a nonspecific action on Epac2, which is different from an observation made using an in vitro assay with purified proteins (Schwede et al., 2015b).

Glucose and forskolin induce membrane potential–independent $[Ca^{2+}]_i$ transients in δ-cells

The final sections deal with the relationship between δ-cell membrane potential and $[Ca^{2+}]_i$ dynamics (Figs. 12, 13, and 14). The finding that tolbutamide is a weaker stimulus of somatostatin secretion than glucose, despite the two compounds having

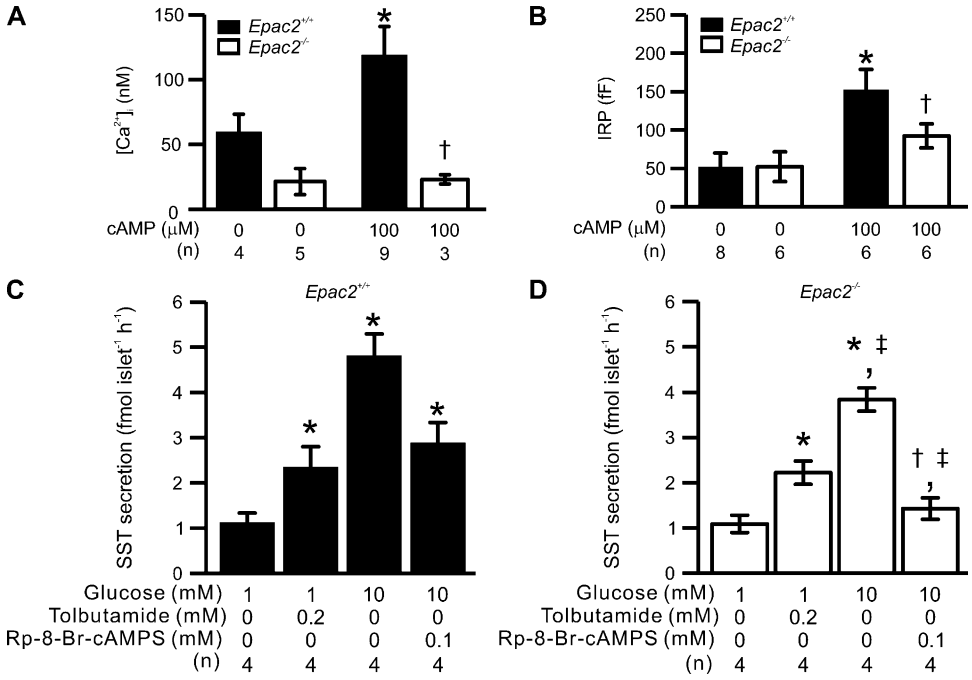

Figure 11. **Ablation of Epac2 (*Rapgef4*) reduces depolarization-triggered $[Ca^{2+}]_i$, exocytosis and GISS in δ-cells.** Somatostatin secretion, depolarization-triggered $[Ca^{2+}]_i$ increases, and exocytosis in Epac2-deficient δ-cells. **(A)** Summary of basal $[Ca^{2+}]_i$ measured in the presence and absence of 100 µM cAMP in δ-cells from control (*Epac2*$^{+/+}$, filled bars) and Epac2 KO (*Epac2*$^{-/-}$, open bars) mice. *, P < 0.05 vs. basal $[Ca^{2+}]_i$ measured in δ-cells without cAMP of the same genotype; †, P < 0.05 vs. basal $[Ca^{2+}]_i$ measured in *Epac2*$^{+/+}$ δ-cells infused with 100 µM cAMP. **(B)** Summary of IRP determined in *Epac2*$^{+/+}$ (filled bars) and *Epac2*$^{-/-}$ (open bars) δ-cells with treatments as indicated below. *, P < 0.05 vs. IRP measured in δ-cells without cAMP of the same genotype; †, P < 0.05 vs. IRP measured in *Epac2*$^{+/+}$ δ-cells infused with 100 µM cAMP. **(C and D)** Somatostatin secretion measured in islets from *Epac2*$^{+/+}$ (C, filled bars) and *Epac2*$^{-/-}$ mice (D, open bars) under the indicated experimental conditions. *, P < 0.05 vs. 1 mM glucose alone of the same genotype; †, P < 0.05 vs. tolbutamide alone of the same genotype; ‡, P < 0.05 vs. responses under the same condition in *Epac2*$^{+/+}$ islets. In A–D, data are presented as mean values ± SEM of indicated numbers of independent experiments (n) from two to six animals for each experimental condition. In A and B, experiments were conducted using the standard whole-cell technique.

similar effects on δ-cell AP firing, suggests that the relationship between electrical activity and exocytosis is complex. To explore this aspect further, we performed parallel measurements of glucose-induced electrical activity and $[Ca^{2+}]_i$ in δ-cells. These experiments were performed by perforated patch membrane potential recordings in δ-cells from SST-GCaMP3 mice.

Consistent with the data in Fig. 1, elevation of glucose from 1 mM to 10 mM produced membrane depolarization and initiated regenerative electrical activity in δ-cells (Fig. 12 A). Interestingly, $[Ca^{2+}]_i$ oscillations measured in parallel did not show a strong correlation to electrical activity (Fig. 12 B). In fact, in 36% of the cells recorded (4 of 11 cells), $[Ca^{2+}]_i$ oscillations preceded glucose-induced AP firing. Furthermore, in the presence of high glucose, the majority of $[Ca^{2+}]_i$ spikes (63 ± 12%; n = 4 cells from four animals) could not be attributed to any preceding APs (Fig. 12 B, *i*).

We classified the $[Ca^{2+}]_i$ spikes into "triggered" (highlighted in red in Fig. 12, A and B) and "spontaneous" events (black), according to the time delay between the $[Ca^{2+}]_i$ spike and the nearest preceding APs (see Materials and methods). The amplitude and duration of the "spontaneous" and "triggered" $[Ca^{2+}]_i$ spikes in high glucose were very variable, and although the "spontaneous" events tended to be smaller, this difference did not attain statistical significance (Fig. 12 C). Upon washout of glucose, $[Ca^{2+}]_i$ spikes were reduced in amplitude (Fig. 12 D) and demonstrated a stronger correlation with the residual APs, with the majority of the events being "triggered" (62 ± 12%; Fig. 12 B, *ii*). The mechanism behind this "hysteresis" remains to be elucidated.

Membrane potential–independent δ-cell $[Ca^{2+}]_i$ spikes involve Epac2 and are sensitive to thapsigargin

The above data indicate that δ-cell $[Ca^{2+}]_i$ spikes induced by high glucose cannot be attributable to AP-mediated Ca^{2+} influx through opening of voltage-gated Ca^{2+} channels alone. To characterize the glucose effect on membrane potential–independent $[Ca^{2+}]_i$ spikes, we measured $[Ca^{2+}]_i$ in SST-GCaMP3 δ-cells that were voltage clamped at V_m (−70 mV) to eliminate AP firing. This series of experiments was also conducted using the perforated patch whole-cell voltage-clamping technique to preserve metabolism.

In δ-cells voltage clamped at −70 mV, glucose (20 mM) remained capable of inducing $[Ca^{2+}]_i$ spikes (Fig. 13 A). These $[Ca^{2+}]_i$ spikes reflect Ca^{2+} release from the ER and were not seen in δ-cells in islets pretreated with thapsigargin (Fig. 13 B). The glucose-induced $[Ca^{2+}]_i$ spikes in voltage-clamped δ-cells were also abolished in islets pretreated with ESI-05, which exerted a thapsigargin-like effect (Fig. 13 C). By contrast, the spontaneous spikes persisted after pretreatment with PKI (Fig. 13 D).

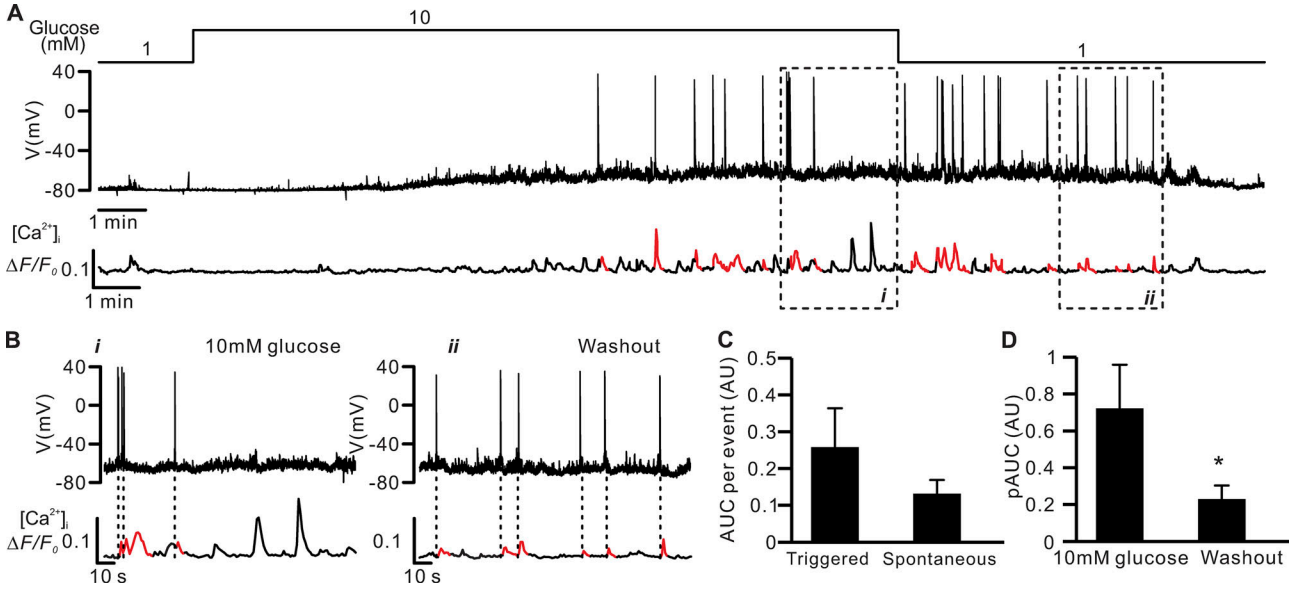

Figure 12. **Electrical activity and $[Ca^{2+}]_i$ in δ-cells.** Poor temporal correlation between δ-cell action potential firing and $[Ca^{2+}]_i$ dynamics. **(A)** Electrical activity (V_m, middle) and changes in $[Ca^{2+}]_i$ (ΔF/F0; bottom) measured simultaneously from an SST-GCaMP3 δ-cell at 1 mM and 10 mM glucose (top). $[Ca^{2+}]_i$ transients temporally correlated to action potentials are highlighted in red ("triggered" events). **(B)** Segments of the recording in A in the presence of 10 mM glucose (*i*) and after its washout (*ii*) displayed on an expanded time scale. Dotted vertical lines indicate $[Ca^{2+}]_i$ spikes that correlated with action potentials. Representative of four similar independent experiments in four different islets from four mice. **(C)** Average integrated $[Ca^{2+}]_i$ transients (AUC) of triggered (139 events in nine independent experiments) and spontaneous events (241 events in nine independent experiments). **(D)** Average spike amplitude of $[Ca^{2+}]_i$ transients (pAUC) when islets were superfused with 10 mM glucose (54 events in four independent experiments) and during the washing out of the glucose stimulus (14 events in four independent experiments). *, $P < 0.05$ vs. 10 mM glucose. In C and D, data are presented as mean values ± SEM. All experiments were conducted using perforated patch whole-cell technique.

Finally, consistent with the data in Fig. 7 E, elevating intracellular cAMP level with a high concentration of forskolin (10 µM) exerted a glucose-like effect on δ-cell $[Ca^{2+}]_i$, an effect that did not correlate with membrane depolarization and AP firing (Fig. 14 A). Like the spontaneous glucose-induced $[Ca^{2+}]_i$ spikes in hyperpolarized δ-cells (Fig. 13 A), the $[Ca^{2+}]_i$ spikes evoked by forskolin were sensitive to thapsigargin (Fig. 14 B).

Discussion

The central role of somatostatin as a key regulator of pancreatic islet function is becoming increasingly evident (Zhang et al., 2014a; van der Meulen et al., 2015; Li et al., 2017, 2018). Somatostatin is a powerful intra-islet inhibitor of insulin and glucagon secretion. Somatostatin receptor antagonists could restore counterregulatory glucagon secretion at low glucose in diabetic rats but not in healthy rats, suggesting an increased intra-islet somatostatin paracrine tone in diabetes (Yue et al., 2012). Studies on the normal regulation of somatostatin secretion may help to understand how it becomes perturbed in diabetes. However, the exact mechanisms regulating somatostatin secretion remain largely unknown (Rorsman and Huising, 2018). This is mainly due to the scarcity of δ-cells (Brissova et al., 2005), making it difficult to perform quantitative measurements. Recently, it has become possible to generate transgenic mice in which fluorescent proteins are specifically expressed in the δ-cells (e.g., SST-tdRFP and SST-GCaMP3 mice). Access to these models allows more detailed analysis of δ-cells gene expression and function (including the mechanisms that control somatostatin release; Chera et al., 2014; van der Meulen et al., 2015; Adriaenssens et al., 2016; DiGruccio et al., 2016). Here we have studied somatostatin secretion, δ-cell electrophysiology, and intracellular Ca^{2+} dynamics using intact mouse pancreatic islets. We demonstrate that glucose stimulates somatostatin secretion from pancreatic δ-cells through both membrane potential–dependent ("V_m-dependent") and –independent ("V_m-independent") pathways.

The V_m-dependent and -independent pathways of glucose-induced somatostatin secretion and their interrelationship are summarized in Fig. 15.

Evidence for V_m-dependent and -independent regulation of GISS

The V_m-dependent pathway largely resembles that of β-cells (Rorsman and Ashcroft, 2018) and involves glucose-induced closure of K_{ATP} channels, membrane depolarization, and AP firing (Göpel et al., 2000). Accordingly, the V_m-dependent effect of glucose can be mimicked by the K_{ATP} channel blocker tolbutamide.

However, membrane depolarization per se is a weak stimulus for somatostatin secretion. Supraphysiological concentrations of extracellular K^+ and tolbutamide evoke less somatostatin secretion than high glucose alone (Fig. 1, B and C). It could be argued that the high $[K^+]_o$-induced depolarization underestimates the contribution of electrical activity because it only transiently increases $[Ca^{2+}]_i$ (Fig. 5 A). However, we found that,

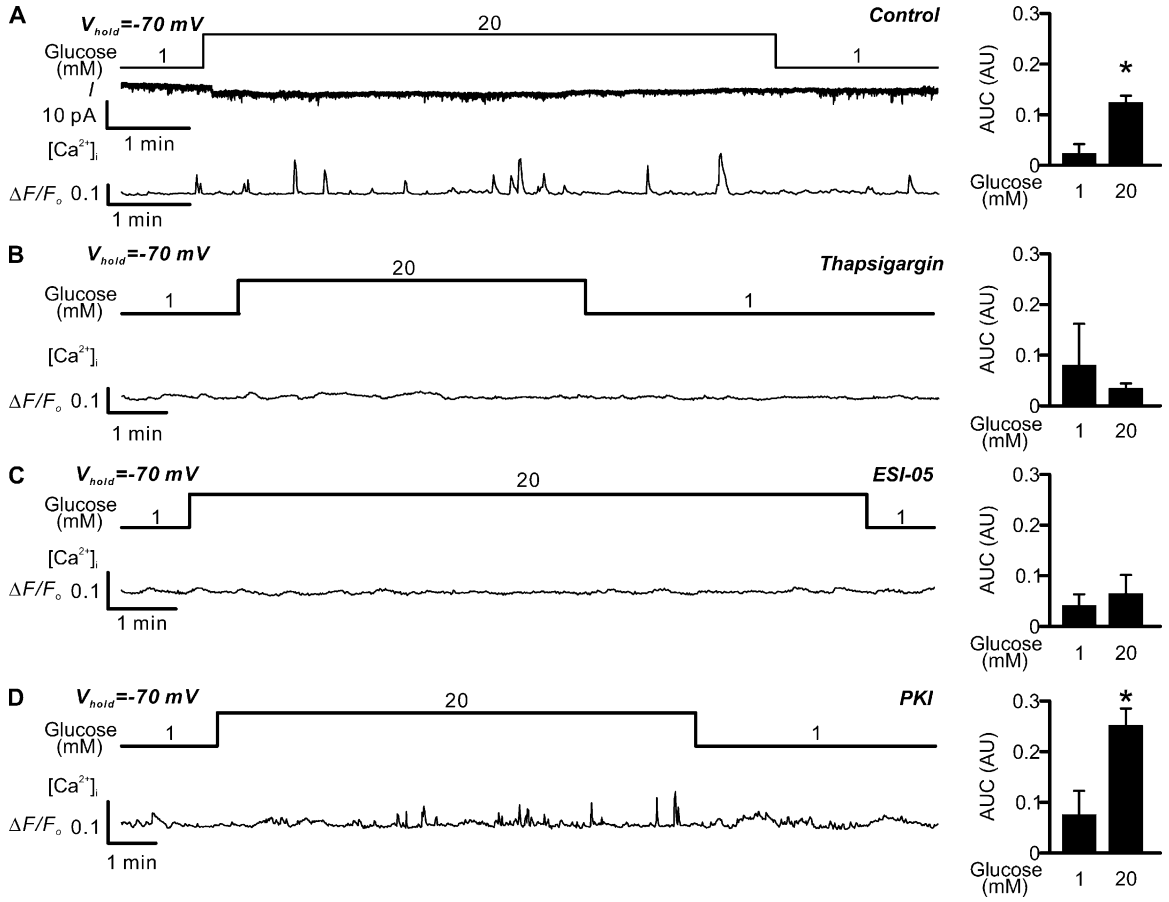

Figure 13. **Glucose-induced $[Ca^{2+}]_i$ oscillations in voltage-clamped δ-cells.** Glucose induces spontaneous Epac2-dependent but PKA-independent $[Ca^{2+}]_i$ spikes in voltage-clamped δ-cells. **(A)** Left: Holding current (*I*; middle) and changes in $[Ca^{2+}]_i$ ($\Delta F/F_0$; bottom) measured in parallel from an SST-GCaMP3 δ-cell voltage-clamped at −70 mV in the presence of 1 mM or 20 mM glucose as indicated (top). Right: Bar graph of the AUCs of $[Ca^{2+}]_i$ at 1 and 20 mM glucose as indicated. Data are presented as mean values ± SEM for six independent experiments with totals of 6 and 34 events at 1 mM and 20 mM glucose, respectively. *, $P < 0.05$ vs. 1 mM glucose. **(B–D)** as in A, but experiments were conducted in islets pretreated with 10 µM thapsigargin (B; three independent experiments with 2 and 17 events at 1 mM and 20 mM glucose, respectively), 25 µM ESI-05 (C; three independent experiments with 8 and 17 events at 1 mM and 20 mM glucose, respectively), or 1 µM myr-PKI (D, four independent experiments with 5 and 20 events at 1 mM and 20 mM glucose, respectively). All experiments were conducted using perforated patch whole-cell technique.

although tolbutamide has an effect on δ-cell electrical activity comparable to that of glucose, it is a much weaker stimulus for somatostatin secretion than glucose (Fig. 1 A and Table 1). This suggests that glucose, in addition to the V_m-dependent effect described above, also exerts a V_m-independent amplifying effect. The identity of the intracellular signals underlying this amplification and links to elevation of glucose has not been established, but the data presented here implicate cAMP. A role for cAMP in the V_m-independent effect of glucose is suggested by the following three observations: (1) glucose increases intracellular cAMP, (2) the adenylyl cyclase activator forskolin and cAMP analogues mimic the amplifying effect of glucose, and (3) the glucose-induced amplifying effect is stimulated by GLP-1 and reduced by inhibitors of the cAMP effectors PKA and Epac2.

cAMP mediates the V_m-independent effect on GISS by stimulating δ-cell ER Ca^{2+} release

Given the importance of cAMP in somatostatin secretion, it is important to consider the mechanism(s) by which glucose increases δ-cell $[cAMP]_i$. In a clonal β-cell line (INS-1E), glucose-stimulated cAMP production was attributed to a Ca^{2+}-activated soluble adenylyl cyclase (adenylyl cyclase 10), which is sensitive to ATP, Ca^{2+}, and bicarbonate (Ramos et al., 2008). However, this is unlikely to be the case in δ-cells because the most abundantly expressed adenylyl cyclase in mouse δ-cells is adenylyl cyclase 6 (Adriaenssens et al., 2016; DiGruccio et al., 2016), which is inhibited by Ca^{2+} (Guillou et al., 1999). We argue that glucose-stimulated cAMP production in δ-cells is secondary to glucose metabolism, rather than a V_m-dependent effect, based on the following two observations: (1) glucose evoked Epac2-dependent $[Ca^{2+}]_i$ oscillations in δ-cells voltage clamped at V_m, and (2) somatostatin secretion evoked by high $[K^+]_o$-triggered depolarization in the absence of glucose/forskolin is not sensitive to antagonists of PKA or Epac2. Therefore, it is likely that elevation in ATP, produced by glucose metabolism, increases substrate availability for cAMP production by adenylyl cyclase in glucose-stimulated δ-cells, a mechanism that is similar to what has been described in β-cells (Dyachok et al., 2008).

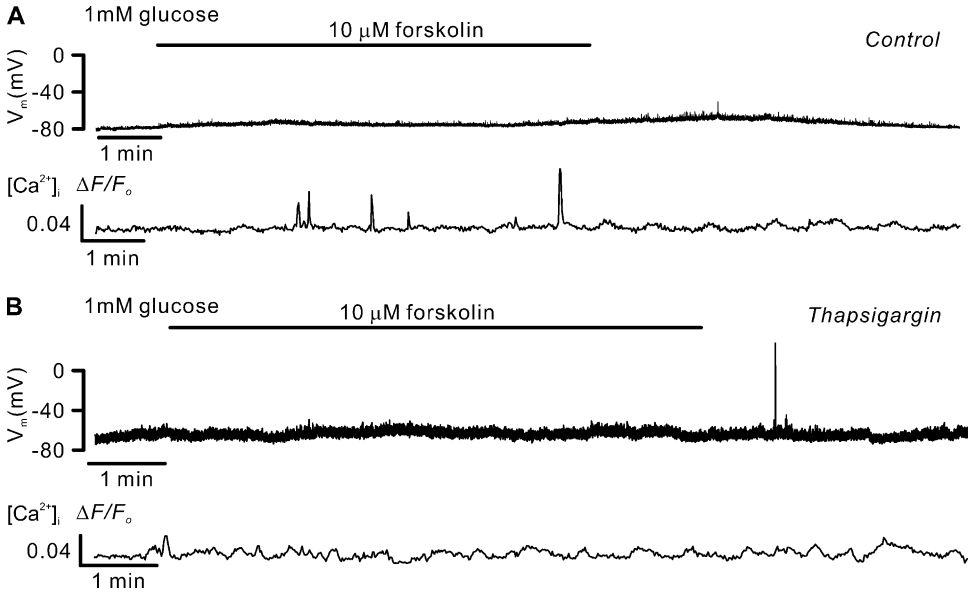

Figure 14. **Forskolin-induced $[Ca^{2+}]_i$ oscillations without δ-cell electrical activity.** Forskolin induces spontaneous $[Ca^{2+}]_i$ spikes sensitive to thapsigargin. **(A)** Membrane potential (V_m, middle) and changes in $[Ca^{2+}]_i$ ($\Delta F/F_0$; bottom) measured simultaneously from an SST-GCaMP3 δ-cell in the absence and presence of 10 μM forskolin. Representative of five independent experiments from three animals. Addition of forskolin is indicted by the horizontal bar. **(B)** As in A, but in δ-cells pretreated with thapsigargin (10 μM) for >1 h. Representative of three independent experiments from three animals. All experiments were conducted using the perforated patch whole-cell technique.

Indeed, the amplifying effect of glucose is reduced by the glucokinase inhibitor mannoheptulose (Fig. 6, A and B; Zhang et al., 2007).

Is the glucose-induced increase in cAMP sufficient to explain the amplifying effect of glucose on somatostatin secretion in δ-cells? Islets exposed to 10 mM glucose produced ∼3 fmol/islet cAMP (Fig. 2 D), similar to what was reported previously by others (Hellman et al., 1974; Eddlestone et al., 1985; Lambillotte et al., 1997; Kimple et al., 2008; Mourad et al., 2012). Given that the intracellular volume of a mouse islet is 1.75 nl (Cooper et al., 1973) and assuming that glucose increases cAMP uniformly in β- and δ-cells (which together comprise 80–85% of the islet cells; Brissova et al., 2002, 2005), we estimate that glucose elevates the intracellular cAMP concentration to ∼2 μM in δ-cells. The latter assumption seems justified given that the optical cAMP measurements showed that the responses in δ- and non–δ-cells were almost superimposable. It has been reported that glucose suppresses cAMP production in α-cells (Elliott et al., 2015; Yu et al., 2019; but see Tian et al., 2011). However, given their low number in the islets (15–20% of the islet cells), the contribution of α-cells in total islet cAMP production is relatively small, and the noise introduced into the above estimate should be insignificant. This estimate is close to that producing the half-maximal increase in δ-cell $[Ca^{2+}]_i$ and exocytosis (3 μM; Fig. 7, C and D). It is also possible that glucose-stimulated cAMP production in δ-cells is compartmentalized and the local concentration of the second messenger is underestimated. Such localized increases in cytoplasmic cAMP have been reported in neurons (Averaimo et al., 2016) and in ventricular myocytes (Surdo et al., 2017).

How does cAMP mediate the V_m-independent effect on somatostatin secretion? Accumulating evidence indicates that Ca^{2+} release from the ER represents a key signal for somatostatin secretion (Zhang et al., 2007; Li et al., 2017; Vierra et al., 2018). The cAMP-mediated amplifying effect of glucose on somatostatin secretion is likely to be exerted, at least partially, by augmenting ER Ca^{2+} release in δ-cells. This is supported by the observations that (1) blocking cAMP effectors (PKA/Epac2) with PKI/ESI-05 and inhibiting ER Ca^{2+} release (with ryanodine) inhibited GISS; and (2) increasing $[cAMP]_i$ with forskolin significantly enhanced depolarization-triggered $[Ca^{2+}]_i$ and exocytotic response. This also correlated with the occurrence of spontaneous $[Ca^{2+}]_i$ spikes, which were induced in voltage-clamped δ-cells by high glucose (20 mM) or forskolin in perforated patch whole-cell measurements (Figs. 7 E, 13 A, and 14) or intracellular application of cAMP (≥10 μM) or the Epac2 agonist 2′-O-Me-cAMP in standard whole-cell recordings (Figs. 8 and 10). The observation that these spikes, in addition to being maintained in voltage-clamped cells, were abolished by thapsigargin suggests they reflect mobilization of intracellular Ca^{2+} release from the ER. These spontaneous $[Ca^{2+}]_i$ spikes may account for the paradox that GISS was not inhibited by pharmacological membrane hyperpolarization by the K_{ATP} channel activator diazoxide in some studies (Zhang et al., 2007; but see van der Meulen et al., 2015). The forskolin-induced $[Ca^{2+}]_i$ oscillations may account for the capacity of high concentrations of forskolin (10 μM) to stimulate somatostatin secretion at 1 mM glucose (De Marinis et al., 2010), an effect that was not associated with δ-cell electrical activity (Fig. 14 A). It may be speculated that the PKA- and Epac2-dependent pathways mediate the stimulatory effects of other cAMP-elevating factors such as GLP-1 (Fig. 3 D), ghrelin (Adriaenssens et al., 2016; DiGruccio et al., 2016) and urocortin 3 (van der Meulen et al., 2015) on somatostatin secretion.

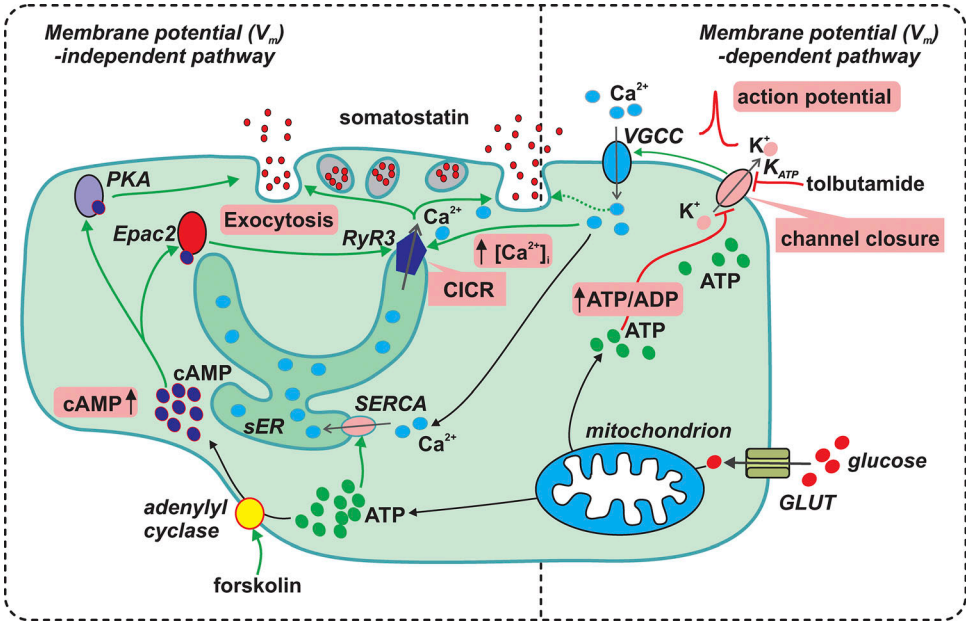

Figure 15. **Glucose stimulates somatostatin secretion through both membrane potential-dependent and -independent pathways.** Membrane potential (V_m)–dependent pathway: glucose (large red particles) metabolism increases δ-cell intracellular ATP (green particles) at the expense of ADP and consequently inhibits the K_{ATP} channels (sensitive to tolbutamide). This leads to membrane depolarization and increase in electrical activity that opens voltage-gated Ca^{2+} channels (VGCC) to allow influx of extracellular Ca^{2+} (blue particles) to increase $[Ca^{2+}]_i$. This exerts a relatively weak stimulation on δ-cell exocytosis (dotted line). V_m-independent pathway: high glucose stimulates somatostatin secretion by promoting CICR in δ-cells. First, the glucose-induced stimulation of ATP production increases ER luminal Ca^{2+} content through SERCA pump. Second, glucose metabolism elevates $[cAMP]_i$ (dark blue particles), a second messenger which activates PKA and Epac2. Whereas PKA directly potentiates δ-cell exocytosis, the effect of Epac2 on exocytosis is mediated through the activation of RYR3 and sensitization of CICR. The cAMP-dependent effects are mimicked by the adenylyl cyclase activator forskolin. The V_m-dependent and -independent pathways operate synergistically leading to a full stimulatory effect of somatostatin secretion by glucose. The key events (increase in ATP/ADP ratio, K_{ATP} channel closure, action potential firing, increase in $[cAMP]_i$, CICR, increase in $[Ca^{2+}]_i$, and exocytosis) are highlighted in pink boxes. Green arrows indicate stimulation, and the red blind-ended arrows indicate inhibition. sER, smooth endoplasmic reticulum; GLUT, glucose transporter.

Differential roles of PKA and Epac2 in GISS

Importantly, although the effects of inhibiting PKA (using PKI) and Epac2 (using ESI-05) on GISS were similar and nonadditive (Figs. 3 and 4), the more detailed single-cell analyses suggest that they are not identical. Thus, PKI (unlike ESI-05) did not affect the cAMP-induced increase in $[Ca^{2+}]_i$ in voltage-clamped δ-cells. This suggests that there is a hierarchy of the PKA- and Epac2-mediated effects: Epac2 is tightly linked to intracellular Ca^{2+} release, whereas PKA may act at the level of exocytosis by effects similar to those documented in pancreatic α- (Gromada et al., 1997) and β-cells (Ammälä et al., 1993). The concept that Epac2 is linked to Ca^{2+} release is supported by the observation that activating Epac2 alone was sufficient to trigger spontaneous $[Ca^{2+}]_i$ oscillations and elevate basal $[Ca^{2+}]_i$ in δ-cells (Fig. 10, B and E). It is therefore of interest that Epac2 has been reported to increase the opening probability of intracellular Ca^{2+}-releasing RYR channel in INS-1 cells (Kang et al., 2001) and cardiomyocytes (Pereira et al., 2007). The latter effect on cardiomyocytes has been attributed to activation of CaMK II, which is downstream of the activation of phospholipase Cε (PLCε) and PKC (Oestreich et al., 2009). However, it should be noted that PLCε (*Plcel*) is expressed at very low levels (if at all) in δ-cells (DiGruccio et al., 2016). This cAMP-induced increase in RYRs activity in δ-cells may constitute the increase in basal $[Ca^{2+}]_i$ (Fig. 7). Notably, a moderate increase in basal $[Ca^{2+}]_i$ from ∼100 to 240 nM (below the threshold for triggering exocytosis) resulted in an ∼80% increase in depolarization-evoked exocytosis (Fig. 9). We attribute this effect to increased Ca^{2+}-dependent granule priming (Heinemann et al., 1993; Gromada et al., 1999). Will the increased basal $[Ca^{2+}]_i$ also promote CICR through higher ER store-filling? Comparing with the cAMP infusion experiments (Fig. 7), increasing basal $[Ca^{2+}]_i$ without cAMP had a relatively small effect on enhancing the depolarization-triggered exocytosis without promoting post-depolarization secretion (Fig. 9, A and B). This indicates an increase in basal $[Ca^{2+}]_i$ per se is insufficient in promoting CICR. Indeed, depolarization-triggered $[Ca^{2+}]_i$ transients were not significantly affected by acutely elevated basal $[Ca^{2+}]_i$ (Fig. 9, C and D).

In addition, it appears that cAMP can stimulate exocytosis directly by activation of PKA, as suggested by the strong inhibitory effect of PKA blockers on both exocytosis (Fig. 10, A and C) and somatostatin secretion (Fig. 4), even when intracellular Ca^{2+} activity was stimulated (via Epac2 activation). Although PKA has been reported to phosphorylate RYR3 (the RYR expressed in δ-cells; Zhang et al., 2007) and increase its channel activity (Ooashi et al., 2005), it appears that such an effect is less important in δ-cells as PKI did not affect intracellular Ca^{2+} release (Fig. 10 F and Fig. 13 D) or the increase in basal $[Ca^{2+}]_i$ (Fig. 10 B). This hypothesis is further supported by the effects of genetic ablation of Epac2: in Epac2-deficient δ-cells, cAMP failed

to increase $[Ca^{2+}]_i$ and stimulate exocytosis, while GISS was abolished by the PKA inhibitor Rp-8-Br-cAMPS (Fig. 11).

cAMP-independent effects on V_m-independent GISS

The finding that cAMP mediates part of the V_m-independent effect of glucose does not exclude the contribution of other mechanisms. It is noteworthy that whereas the forskolin stimulatory effect on depolarization-evoked somatostatin secretion was nearly abolished by PKI and ESI-05, part of the effect of glucose was resistant to these inhibitors (Fig. 4, A and B). It is possible that glucose mediates this effect by promoting Ca^{2+} uptake into the intracellular Ca^{2+} stores (Fig. 6, C and D). Thus, the increase in δ-cell exocytosis at high glucose correlates with the high level of Ca^{2+} available for release from the ER (Fig. 6, E and F). This may also explain the observation that blocking the RYR or the R-type Ca^{2+} channel (the two key components for δ-cell CICR) had no inhibitory effect on high $[K^+]_o$-triggered somatostatin secretion in the absence of glucose (Zhang et al., 2007).

Full magnitude GISS requires both V_m-dependent and -independent pathways

How do the V_m-dependent and -independent pathways contribute to GISS? When intracellular cAMP is low (at low glucose), isolated opening of R-type Ca^{2+} channels is insufficient to trigger CICR and the full secretory response. This accounts for the low amplitude of the depolarization-evoked $[Ca^{2+}]$ transients in the absence of cAMP (Fig. 7 and Table 2) and by the reported lack of effect of the R-type Ca^{2+} channel blocker SNX-482 on high $[K^+]_o$-stimulated somatostatin secretion in the absence of glucose (Zhang et al., 2007). On the other hand, without membrane depolarization/activation of voltage-gated Ca^{2+} channels, elevating intracellular cAMP (with forskolin) alone had only a weak stimulatory effect on somatostatin secretion (De Marinis et al., 2010), despite the increase in spontaneous ER Ca^{2+} release (Fig. 14 A). Therefore, the synergistic effects of membrane depolarization, opening of R-type Ca^{2+} channels and cAMP-dependent ER Ca^{2+} release are required for glucose to exert its full stimulatory effect on somatostatin secretion.

Coda

It is clear that the regulation of hormone secretion from δ- and β-cells exhibits many similarities. Both processes involve V_m-dependent and -independent mechanisms. In insulin-secreting cells, GLP-1 has been shown to induce CICR by a cAMP-dependent mechanism (Gromada et al., 1995; Dzhura et al., 2010). However, the two types of islet cells do differ in several important respects. Whereas modulators of CICR do not affect glucose-induced insulin secretion from mouse β-cells, CICR plays a central role in glucose-stimulated somatostatin secretion from δ-cells (Zhang et al., 2007). This study identifies cAMP and activation of Epac2 as a critical link between glucose metabolism and δ-cell CICR. This explains the observation that the δ-cell electrical activity appears to play a less decisive role in somatostatin secretion and that the V_m-independent pathways can maintain somatostatin secretion even in the absence of regenerative electrical activity. Unlike β- and α-cells, which exhibit spherical geometry, the δ-cells are more complex. In addition to a cell body, they also possess neurite-like processes that may extend several tens of microns and thereby attain close proximity to several β- or α-cells (Brereton et al., 2015). Future studies with improved genetically encoded Ca^{2+} indicators (such as GCaMP6) may enable the resolution of V_m-independent $[Ca^{2+}]_i$ spikes in these processes, and whether they represent a means by which δ-cells can respond to factors released locally by α- and β-cells and adjust somatostatin secretion accordingly.

Acknowledgments

Eduardo Ríos served as editor.

We dedicate this manuscript to our late colleague Dr. Matthias Braun for most insightful advice during the early stages of this project. We thank F.M. Ashcroft for discussions and comments on the manuscript.

Supported by Diabetes UK (P. Rorsman, Q. Zhang, and R. Ramracheya), the Wellcome Trust (P. Rorsman, grant 095531/Z/11/Z), the NIHR Oxford Biomedical Research Centre (A. Tarasov and P. Rorsman), the Diabetes Research and Wellness Foundation Sweden (A. Salehi), the Knut and Alice Wallenbergs Stiftelse (P. Rorsman), and the Swedish Research Council (P. Rorsman). Q. Zhang is a Diabetes UK RD Lawrence Research fellow (grant DUK-14/0005128).

The authors declare no competing financial interests.

Author contributions: Q. Zhang, G. Denwood, R. Ramracheya, A. Salehi, A. Tarasov, and E. Vergari performed the experiments and analyzed the data. F. Reimann and F. Gribble supplied the SST-Cre mice. S. Seino and H. Takahashi provided *Epac2*$^{-/-}$ mice. V.O. Nikolaev provided the fluorescent cAMP probe (Epac2-camps). Q. Zhang and P. Rorsman planned the experiments and wrote the paper.

Submitted: 18 February 2019
Revised: 11 May 2019
Accepted: 9 July 2019

References

Adriaenssens, A., B.Y.H. Lam, L. Billing, K. Skeffington, S. Sewing, F. Reimann, and F. Gribble. 2015. A Transcriptome-Led Exploration of Molecular Mechanisms Regulating Somatostatin-Producing D-Cells in the Gastric Epithelium. *Endocrinology*. 156:3924–3936. https://doi.org/10.1210/en.2015-1301

Adriaenssens, A.E., B. Svendsen, B.Y.H. Lam, G.S.H. Yeo, J.J. Holst, F. Reimann, and F.M. Gribble. 2016. Transcriptomic profiling of pancreatic alpha, beta and delta cell populations identifies delta cells as a principal target for ghrelin in mouse islets. *Diabetologia*. 59:2156–2165. https://doi.org/10.1007/s00125-016-4033-1

Ammälä, C., F.M. Ashcroft, and P. Rorsman. 1993. Calcium-independent potentiation of insulin release by cyclic AMP in single β-cells. *Nature*. 363:356–358. https://doi.org/10.1038/363356a0

Averaimo, S., A. Assali, O. Ros, S. Couvet, Y. Zagar, I. Genescu, A. Rebsam, and X. Nicol. 2016. A plasma membrane microdomain compartmentalizes ephrin-generated cAMP signals to prune developing retinal axon arbors. *Nat. Commun.* 7:12896. https://doi.org/10.1038/ncomms12896

Barg, S., X. Ma, L. Eliasson, J. Galvanovskis, S.O. Göpel, S. Obermüller, J. Platzer, E. Renström, M. Trus, D. Atlas, et al. 2001. Fast exocytosis with few Ca(2+) channels in insulin-secreting mouse pancreatic B cells. *Biophys. J.* 81:3308–3323. https://doi.org/10.1016/S0006-3495(01)75964-4

Braun, M., R. Ramracheya, S. Amisten, M. Bengtsson, Y. Moritoh, Q. Zhang, P.R. Johnson, and P. Rorsman. 2009. Somatostatin release, electrical activity, membrane currents and exocytosis in human pancreatic delta cells. *Diabetologia*. 52:1566–1578. https://doi.org/10.1007/s00125-009-1382-z

Brereton, M.F., E. Vergari, Q. Zhang, and A. Clark. 2015. Alpha-, Delta- and PP-cells: Are They the Architectural Cornerstones of Islet Structure and Co-ordination? *J. Histochem. Cytochem.* 63:575–591. https://doi.org/10.1369/0022155415583535

Briant, L.J., Q. Zhang, E. Vergari, J.A. Kellard, B. Rodriguez, F.M. Ashcroft, and P. Rorsman. 2017. Functional identification of islet cell types by electrophysiological fingerprinting. *J. R. Soc. Interface.* 14:20160999. https://doi.org/10.1098/rsif.2016.0999

Brissova, M., M. Shiota, W.E. Nicholson, M. Gannon, S.M. Knobel, D.W. Piston, C.V.E. Wright, and A.C. Powers. 2002. Reduction in pancreatic transcription factor PDX-1 impairs glucose-stimulated insulin secretion. *J. Biol. Chem.* 277:11225–11232. https://doi.org/10.1074/jbc.M111272200

Brissova, M., M.J. Fowler, W.E. Nicholson, A. Chu, B. Hirshberg, D.M. Harlan, and A.C. Powers. 2005. Assessment of human pancreatic islet architecture and composition by laser scanning confocal microscopy. *J. Histochem. Cytochem.* 53:1087–1097. https://doi.org/10.1369/jhc.5C6684.2005

Cabrera, O., D.M. Berman, N.S. Kenyon, C. Ricordi, P.-O. Berggren, and A. Caicedo. 2006. The unique cytoarchitecture of human pancreatic islets has implications for islet cell function. *Proc. Natl. Acad. Sci. USA.* 103:2334–2339. https://doi.org/10.1073/pnas.0510790103

Cejvan, K., D.H. Coy, and S. Efendic. 2003. Intra-islet somatostatin regulates glucagon release via type 2 somatostatin receptors in rats. *Diabetes.* 52:1176–1181. https://doi.org/10.2337/diabetes.52.5.1176

Cheng-Xue, R., A. Gómez-Ruiz, N. Antoine, L.A. Noël, H.Y. Chae, M.A. Ravier, F. Chimienti, F.C. Schuit, and P. Gilon. 2013. Tolbutamide controls glucagon release from mouse islets differently than glucose: involvement of K(ATP) channels from both α-cells and δ-cells. *Diabetes.* 62:1612–1622. https://doi.org/10.2337/db12-0347

Chera, S., D. Baronnier, L. Ghila, V. Cigliola, J.N. Jensen, G. Gu, K. Furuyama, F. Thorel, F.M. Gribble, F. Reimann, and P.L. Herrera. 2014. Diabetes recovery by age-dependent conversion of pancreatic δ-cells into insulin producers. *Nature.* 514:503–507. https://doi.org/10.1038/nature13633

Cooper, R.H., S.J. Ashcroft, and P.J. Randle. 1973. Concentration of adenosine 3′:5′-cyclic monophosphate in mouse pancreatic islets measured by a protein-binding radioassay. *Biochem. J.* 134:599–605. https://doi.org/10.1042/bj1340599

De Marinis, Y.Z., A. Salehi, C.E. Ward, Q. Zhang, F. Abdulkader, M. Bengtsson, O. Braha, M. Braun, R. Ramracheya, S. Amisten, et al. 2010. GLP-1 inhibits and adrenaline stimulates glucagon release by differential modulation of N- and L-type Ca2+ channel-dependent exocytosis. *Cell Metab.* 11:543–553. https://doi.org/10.1016/j.cmet.2010.04.007

DiGruccio, M.R., A.M. Mawla, C.J. Donaldson, G.M. Noguchi, J. Vaughan, C. Cowing-Zitron, T. van der Meulen, and M.O. Huising. 2016. Comprehensive alpha, beta and delta cell transcriptomes reveal that ghrelin selectively activates delta cells and promotes somatostatin release from pancreatic islets. *Mol. Metab.* 5:449–458. https://doi.org/10.1016/j.molmet.2016.04.007

Dyachok, O., O. Idevall-Hagren, J. Sågetorp, G. Tian, A. Wuttke, C. Arrieumerlou, G. Akusjärvi, E. Gylfe, and A. Tengholm. 2008. Glucose-induced cyclic AMP oscillations regulate pulsatile insulin secretion. *Cell Metab.* 8:26–37. https://doi.org/10.1016/j.cmet.2008.06.003

Dzhura, I., O.G. Chepurny, G.G. Kelley, C.A. Leech, M.W. Roe, E. Dzhura, P. Afshari, S. Malik, M.J. Rindler, X. Xu, et al. 2010. Epac2-dependent mobilization of intracellular Ca^{2+} by glucagon-like peptide-1 receptor agonist exendin-4 is disrupted in β-cells of phospholipase C-ε knockout mice. *J. Physiol.* 588:4871–4889. https://doi.org/10.1113/jphysiol.2010.198424

Eddlestone, G.T., S.B. Oldham, L.G. Lipson, F.H. Premdas, and P.M. Beigelman. 1985. Electrical activity, cAMP concentration, and insulin release in mouse islets of Langerhans. *Am. J. Physiol.* 248:C145–C153. https://doi.org/10.1152/ajpcell.1985.248.1.C145

Elliott, A.D., A. Ustione, and D.W. Piston. 2015. Somatostatin and insulin mediate glucose-inhibited glucagon secretion in the pancreatic α-cell by lowering cAMP. *Am. J. Physiol. Endocrinol. Metab.* 308:E130–E143. https://doi.org/10.1152/ajpendo.00344.2014

Göpel, S., T. Kanno, S. Barg, J. Galvanovskis, and P. Rorsman. 1999. Voltage-gated and resting membrane currents recorded from B-cells in intact mouse pancreatic islets. *J. Physiol.* 521:717–728. https://doi.org/10.1111/j.1469-7793.1999.00717.x

Göpel, S.O., T. Kanno, S. Barg, and P. Rorsman. 2000. Patch-clamp characterisation of somatostatin-secreting δ-cells in intact mouse pancreatic islets. *J. Physiol.* 528:497–507. https://doi.org/10.1111/j.1469-7793.2000.00497.x

Göpel, S., Q. Zhang, L. Eliasson, X.S. Ma, J. Galvanovskis, T. Kanno, A. Salehi, and P. Rorsman. 2004. Capacitance measurements of exocytosis in mouse pancreatic alpha-, beta- and delta-cells within intact islets of Langerhans. *J. Physiol.* 556:711–726. https://doi.org/10.1113/jphysiol.2003.059675

Gromada, J., S. Dissing, K. Bokvist, E. Renström, J. Frøkjaer-Jensen, B.S. Wulff, and P. Rorsman. 1995. Glucagon-like peptide I increases cytoplasmic calcium in insulin-secreting β TC3-cells by enhancement of intracellular calcium mobilization. *Diabetes.* 44:767–774. https://doi.org/10.2337/diab.44.7.767

Gromada, J., K. Bokvist, W.G. Ding, S. Barg, K. Buschard, E. Renström, and P. Rorsman. 1997. Adrenaline stimulates glucagon secretion in pancreatic A-cells by increasing the Ca2+ current and the number of granules close to the L-type Ca2+ channels. *J. Gen. Physiol.* 110:217–228. https://doi.org/10.1085/jgp.110.3.217

Gromada, J., M. Høy, E. Renström, K. Bokvist, L. Eliasson, S. Göpel, and P. Rorsman. 1999. CaM kinase II-dependent mobilization of secretory granules underlies acetylcholine-induced stimulation of exocytosis in mouse pancreatic B-cells. *J. Physiol.* 518:745–759. https://doi.org/10.1111/j.1469-7793.1999.0745p.x

Guillou, J.-L., H. Nakata, and D.M.F. Cooper. 1999. Inhibition by calcium of mammalian adenylyl cyclases. *J. Biol. Chem.* 274:35539–35545. https://doi.org/10.1074/jbc.274.50.35539

Gylfe, E., and P. Gilon. 2014. Glucose regulation of glucagon secretion. *Diabetes Res. Clin. Pract.* 103:1–10. https://doi.org/10.1016/j.diabres.2013.11.019

Hamilton, A., Q. Zhang, A. Salehi, M. Willems, J.G. Knudsen, A.K. Ringgaard, C.E. Chapman, A. Gonzalez-Alvarez, N.C. Surdo, M. Zaccolo, et al. 2018. Adrenaline Stimulates Glucagon Secretion by Tpc2-Dependent Ca^{2+} Mobilization From Acidic Stores in Pancreatic α-Cells. *Diabetes.* 67:1128–1139. https://doi.org/10.2337/db17-1102

Hauge-Evans, A.C., A.J. King, D. Carmignac, C.C. Richardson, I.C. Robinson, M.J. Low, M.R. Christie, S.J. Persaud, and P.M. Jones. 2009. Somatostatin secreted by islet delta-cells fulfills multiple roles as a paracrine regulator of islet function. *Diabetes.* 58:403–411. https://doi.org/10.2337/db08-0792

Heinemann, C., L. von Rüden, R.H. Chow, and E. Neher. 1993. A two-step model of secretion control in neuroendocrine cells. *Pflugers Arch.* 424:105–112. https://doi.org/10.1007/BF00374600

Hellman, B., L.A. Idahl, A. Lernmark, and I.B. Täljedal. 1974. The pancreatic beta-cell recognition of insulin secretagogues: does cyclic AMP mediate the effect of glucose? *Proc. Natl. Acad. Sci. USA.* 71:3405–3409. https://doi.org/10.1073/pnas.71.9.3405

Kang, G., O.G. Chepurny, and G.G. Holz. 2001. cAMP-regulated guanine nucleotide exchange factor II (Epac2) mediates Ca2+-induced Ca2+ release in INS-1 pancreatic beta-cells. *J. Physiol.* 536:375–385. https://doi.org/10.1111/j.1469-7793.2001.0375c.xd

Kanno, T., X. Ma, S. Barg, L. Eliasson, J. Galvanovskis, S. Göpel, M. Larsson, E. Renström, and P. Rorsman. 2004. Large dense-core vesicle exocytosis in pancreatic beta-cells monitored by capacitance measurements. *Methods.* 33:302–311. https://doi.org/10.1016/j.ymeth.2004.01.003

Kimple, M.E., J.W. Joseph, C.L. Bailey, P.T. Fueger, I.A. Hendry, C.B. Newgard, and P.J. Casey. 2008. Galphaz negatively regulates insulin secretion and glucose clearance. *J. Biol. Chem.* 283:4560–4567. https://doi.org/10.1074/jbc.M706481200

Lambillotte, C., P. Gilon, and J.C. Henquin. 1997. Direct glucocorticoid inhibition of insulin secretion. An in vitro study of dexamethasone effects in mouse islets. *J. Clin. Invest.* 99:414–423. https://doi.org/10.1172/JCI119175

Li, N., Z. Yang, Q. Li, Z. Yu, X. Chen, J.-C. Li, B. Li, S.-L. Ning, M. Cui, J.-P. Sun, and X. Yu. 2018. Ablation of somatostatin cells leads to impaired pancreatic islet function and neonatal death in rodents. *Cell Death Dis.* 9:682. https://doi.org/10.1038/s41419-018-0741-4

Li, Q., M. Cui, F. Yang, N. Li, B. Jiang, Z. Yu, D. Zhang, Y. Wang, X. Zhu, H. Hu, et al. 2017. A cullin 4B-RING E3 ligase complex fine-tunes pancreatic δ cell paracrine interactions. *J. Clin. Invest.* 127:2631–2646. https://doi.org/10.1172/JCI91348

Mourad, N.I., M. Nenquin, and J.-C. Henquin. 2012. cAMP-mediated and metabolic amplification of insulin secretion are distinct pathways

sharing independence of β-cell microfilaments. *Endocrinology*. 153: 4644–4654. https://doi.org/10.1210/en.2012-1450

Nikolaev, V.O., M. Bünemann, L. Hein, A. Hannawacker, and M.J. Lohse. 2004. Novel single chain cAMP sensors for receptor-induced signal propagation. *J. Biol. Chem.* 279:37215–37218. https://doi.org/10.1074/jbc.C400302200

Oestreich, E.A., S. Malik, S.A. Goonasekera, B.C. Blaxall, G.G. Kelley, R.T. Dirksen, and A.V. Smrcka. 2009. Epac and phospholipase Cepsilon regulate Ca2+ release in the heart by activation of protein kinase Cepsilon and calcium-calmodulin kinase II. *J. Biol. Chem.* 284:1514–1522. https://doi.org/10.1074/jbc.M806994200

Olofsson, C.S., S.O. Göpel, S. Barg, J. Galvanovskis, X. Ma, A. Salehi, P. Rorsman, and L. Eliasson. 2002. Fast insulin secretion reflects exocytosis of docked granules in mouse pancreatic B-cells. *Pflugers Arch.* 444: 43–51. https://doi.org/10.1007/s00424-002-0781-5

Ooashi, N., A. Futatsugi, F. Yoshihara, K. Mikoshiba, and H. Kamiguchi. 2005. Cell adhesion molecules regulate Ca2+-mediated steering of growth cones via cyclic AMP and ryanodine receptor type 3. *J. Cell Biol.* 170: 1159–1167. https://doi.org/10.1083/jcb.200503157

Pereira, L., M. Métrich, M. Fernández-Velasco, A. Lucas, J. Leroy, R. Perrier, E. Morel, R. Fischmeister, S. Richard, J.-P. Bénitah, et al. 2007. The cAMP binding protein Epac modulates Ca2+ sparks by a Ca2+/calmodulin kinase signalling pathway in rat cardiac myocytes. *J. Physiol.* 583:685–694. https://doi.org/10.1113/jphysiol.2007.133066

Ramos, L.S., J.H. Zippin, M. Kamenetsky, J. Buck, and L.R. Levin. 2008. Glucose and GLP-1 stimulate cAMP production via distinct adenylyl cyclases in INS-1E insulinoma cells. *J. Gen. Physiol.* 132:329–338. https://doi.org/10.1085/jgp.200810044

Richards, P., H.E. Parker, A.E. Adriaenssens, J.M. Hodgson, S.C. Cork, S. Trapp, F.M. Gribble, and F. Reimann. 2014. Identification and characterization of GLP-1 receptor-expressing cells using a new transgenic mouse model. *Diabetes.* 63:1224–1233. https://doi.org/10.2337/db13-1440

Rorsman, P., and F.M. Ashcroft. 2018. Pancreatic β-Cell Electrical Activity and Insulin Secretion: Of Mice and Men. *Physiol. Rev.* 98:117–214. https://doi.org/10.1152/physrev.00008.2017

Rorsman, P., and M.O. Huising. 2018. The somatostatin-secreting pancreatic δ-cell in health and disease. *Nat. Rev. Endocrinol.* 14:404–414. https://doi.org/10.1038/s41574-018-0020-6

Rorsman, P., and E. Renström. 2003. Insulin granule dynamics in pancreatic beta cells. *Diabetologia.* 46:1029–1045. https://doi.org/10.1007/s00125-003-1153-1

Rorsman, P., R. Ramracheya, N.J. Rorsman, and Q. Zhang. 2014. ATP-regulated potassium channels and voltage-gated calcium channels in pancreatic alpha and beta cells: similar functions but reciprocal effects on secretion. *Diabetologia.* 57:1749–1761. https://doi.org/10.1007/s00125-014-3279-8

Schwede, F., D. Bertinetti, C.N. Langerijs, M.A. Hadders, H. Wienk, J.H. Ellenbroek, E.J.P. de Koning, J.L. Bos, F.W. Herberg, H.-G. Genieser, et al. 2015a. Structure-guided design of selective Epac1 and Epac2 agonists. *PLoS Biol.* 13:e1002038. https://doi.org/10.1371/journal.pbio.1002038

Schwede, F., O.G. Chepurny, M. Kaufholz, D. Bertinetti, C.A. Leech, O. Cabrera, Y. Zhu, F. Mei, X. Cheng, J.E. Manning Fox, et al. 2015b. Rp-cAMPS Prodrugs Reveal the cAMP Dependence of First-Phase Glucose-Stimulated Insulin Secretion. *Mol. Endocrinol.* 29:988–1005. https://doi.org/10.1210/me.2014-1330

Shibasaki, T., H. Takahashi, T. Miki, Y. Sunaga, K. Matsumura, M. Yamanaka, C. Zhang, A. Tamamoto, T. Satoh, J. Miyazaki, and S. Seino. 2007. Essential role of Epac2/Rap1 signaling in regulation of insulin granule dynamics by cAMP. *Proc. Natl. Acad. Sci. USA.* 104:19333–19338. https://doi.org/10.1073/pnas.0707054104

Surdo, N.C., M. Berrera, A. Koschinski, M. Brescia, M.R. Machado, C. Carr, P. Wright, J. Gorelik, S. Morotti, E. Grandi, et al. 2017. FRET biosensor uncovers cAMP nano-domains at β-adrenergic targets that dictate precise tuning of cardiac contractility. *Nat. Commun.* 8:15031. https://doi.org/10.1038/ncomms15031

Thorens, B. 1992. Expression cloning of the pancreatic beta cell receptor for the gluco-incretin hormone glucagon-like peptide 1. *Proc. Natl. Acad. Sci. USA.* 89:8641–8645. https://doi.org/10.1073/pnas.89.18.8641

Tian, G., S. Sandler, E. Gylfe, and A. Tengholm. 2011. Glucose- and hormone-induced cAMP oscillations in α- and β-cells within intact pancreatic islets. *Diabetes.* 60:1535–1543. https://doi.org/10.2337/db10-1087

Trube, G., P. Rorsman, and T. Ohno-Shosaku. 1986. Opposite effects of tolbutamide and diazoxide on the ATP-dependent K+ channel in mouse pancreatic β-cells. *Pflugers Arch.* 407:493–499. https://doi.org/10.1007/BF00657506

van der Meulen, T., C.J. Donaldson, E. Cáceres, A.E. Hunter, C. Cowing-Zitron, L.D. Pound, M.W. Adams, A. Zembrzycki, K.L. Grove, and M.O. Huising. 2015. Urocortin3 mediates somatostatin-dependent negative feedback control of insulin secretion. *Nat. Med.* 21:769–776. https://doi.org/10.1038/nm.3872

Vierra, N.C., M.T. Dickerson, K.L. Jordan, P.K. Dadi, K.A. Katdare, M.K. Altman, S.C. Milian, and D.A. Jacobson. 2018. TALK-1 reduces delta-cell endoplasmic reticulum and cytoplasmic calcium levels limiting somatostatin secretion. *Mol. Metab.* 9:84–97. https://doi.org/10.1016/j.molmet.2018.01.016

Walker, J.N., R. Ramracheya, Q. Zhang, P.R.V. Johnson, M. Braun, and P. Rorsman. 2011. Regulation of glucagon secretion by glucose: paracrine, intrinsic or both? *Diabetes Obes. Metab.* 13(Suppl 1):95–105. https://doi.org/10.1111/j.1463-1326.2011.01450.x

Yu, Q., H. Shuai, P. Ahooghalandari, E. Gylfe, and A. Tengholm. 2019. Glucose controls glucagon secretion by directly modulating cAMP in alpha cells. *Diabetologia.* 62:1212–1224. https://doi.org/10.1007/s00125-019-4857-6

Yue, J.T., E. Burdett, D.H. Coy, A. Giacca, S. Efendic, and M. Vranic. 2012. Somatostatin receptor type 2 antagonism improves glucagon and corticosterone counterregulatory responses to hypoglycemia in streptozotocin-induced diabetic rats. *Diabetes.* 61:197–207. https://doi.org/10.2337/db11-0690

Zhang, J., L.B. McKenna, C.W. Bogue, and K.H. Kaestner. 2014a. The diabetes gene Hhex maintains δ-cell differentiation and islet function. *Genes Dev.* 28:829–834. https://doi.org/10.1101/gad.235499.113

Zhang, Q., M. Bengtsson, C. Partridge, A. Salehi, M. Braun, R. Cox, L. Eliasson, P.R. Johnson, E. Renström, T. Schneider, et al. 2007. R-type Ca(2+)-channel-evoked CICR regulates glucose-induced somatostatin secretion. *Nat. Cell Biol.* 9:453–460. https://doi.org/10.1038/ncb1563

Zhang, Q., M.V. Chibalina, M. Bengtsson, L.N. Groschner, R. Ramracheya, N.J. Rorsman, V. Leiss, M.A. Nassar, A. Welling, F.M. Gribble, et al. 2014b. Na+ current properties in islet α- and β-cells reflect cell-specific Scn3a and Scn9a expression. *J. Physiol.* 592:4677–4696. https://doi.org/10.1113/jphysiol.2014.274209